STRUCTURAL CHEMISTRY

ISSN 2053-2296

Two polymorph modifications of tris(hexafluoroacetylacetonato)iron(III) revealed: is that common for other trivalent metals?

Joyce Chang, Julianna N. Defeo, Zheng Wei* and Evgeny V. Dikarev*

Department of Chemistry, University at Albany, Albany, New York 12222, USA. *Correspondence e-mail: zwei@albany.edu, edikarev@albany.edu

Received 25 June 2024
Accepted 31 July 2024

Edited by X. Wang, Oak Ridge National Laboratory, USA

Keywords: crystal structure; iron(III) hexafluoroacetylacetonate; tris-chelated; mononuclear complex; phase transformation; fluorinated β-diketonate; polymorph modification; octahedral complex.

CCDC references: 2364188; 2364187

Supporting information: this article has supporting information at journals.iucr.org/c

A long-standing issue about the correct identification of an important starting reagent, iron(III) hexafluoroacetylacetonate, $Fe(hfac)_3$ (**1**), has been resolved. The *tris*-chelated mononuclear complex was found to crystallize in two polymorph modifications which can be assigned as the low-temperature (**1-L**) monoclinic $P2_1/n$ and the high-temperature (**1-H**) trigonal $P\overline{3}$. Low-temperature polymorph **1-L** was found to transform to **1-H** upon sublimation at 44 °C. Two modifications are clearly distinguished by powder X-ray diffraction (PXRD), single-crystal X-ray diffraction, differential scanning calorimetry (DSC), and melting-point measurements. On the other hand, the two forms share similar characteristics in direct analysis in real-time mass spectrometry (DART-MS), attenuated total reflection (ATR) spectroscopy, and some physical properties, such as color, volatility, sensitivity, and solubility. Analysis of the literature and some of our preliminary data strongly suggest that the appearance of two polymorph modifications for trivalent metal (both transition and main group) hexafluoroacetylacetonates is a common case for several largely used complexes not yet accounted for in the crystallographic databases.

1. Introduction

Fluorinated β-diketonates are valued for their high volatility and solubility relative to their corresponding nonfluorinated counterparts (Sievers & Sadlowski, 1978; Fahlman & Barron, 2000; Mishra & Daniele, 2015; Crowder *et al.*, 2019; Smolentsev *et al.*, 2011). Due to their unique properties, the trivalent metal hexafluoroacetylacetonates, $M(hfac)_3$, have been successfully utilized in many fields, such as metal–organic chemical vapor deposition (MOCVD) (Lassègue *et al.*, 2015; Bespalova *et al.*, 2020; Stienen & Bendt, 2020; Dhar *et al.*, 2015; Fahlman & Barron, 2000; Talaga *et al.*, 1998; Ballarin *et al.*, 1994; Battiston *et al.*, 1996; Lee *et al.*, 2001; Zherikova *et al.*, 2013), catalysis (Gostynski *et al.*, 2016; Conradie & Conradie, 2015; Kato & Mukaiyama, 1992; Denmark & Cresswell, 2013; Takai *et al.*, 1991; Neumann & Kochi, 1975; Conradie, 2022; Freitag & Conradie, 2015; Bryant *et al.*, 2002; Chakravarty & Adhikari, 1991; Ma *et al.*, 1999), supercritical carbon dioxide techniques (Peng *et al.*, 2008; Umecky *et al.*, 2011; Opwis *et al.*, 2022), and synthesis (Moxon *et al.*, 1981; Tangwatanakul *et al.*, 2016; Chokprasombat *et al.*, 2014; Drath *et al.*, 2018; Gostynski *et al.*, 2017; Woo *et al.*, 2012; Waidmann *et al.*, 2012; Makhaev & Petrova, 2017).

Over the years, our group has successfully employed $Fe(hfac)_3$ as a starting reagent to synthesize both homo- (Zhang, Li, Sun *et al.*, 2008; Lieberman *et al.*, 2015) and heterometallic (Zhang, Li, Sun *et al.*, 2008; Navulla *et al.*, 2011; Wei *et al.*, 2013; Lieberman *et al.*, 2017; Barry *et al.*, 2018; Han

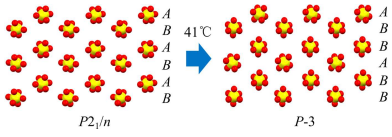

Table 1
Experimental details.

For both determinations: $[Fe(C_5HF_6O_2)_3]$, M_r = 677.02. Experiments were carried out at 100 K. H-atom parameters were constrained.

	1-L	**1-H**
Crystal data		
Crystal system, space group	Monoclinic, $P2_1/n$	Trigonal, $P\overline{3}$
a, b, c (Å)	8.7659 (2), 12.9796 (3), 19.1759 (5)	18.1141 (4), 18.1141 (4), 11.7136 (3)
α, β, γ (°)	90, 91.632 (2), 90	90, 90, 120
V (Å^3)	2180.90 (9)	3328.54 (17)
Z	4	6
Radiation type	Mo $K\alpha$	Synchrotron, λ = 0.41329 Å
μ (mm^{-1})	0.88	0.21
Crystal size (mm)	0.16 × 0.12 × 0.09	0.15 × 0.12 × 0.09
Data collection		
Diffractometer	Rigaku XtaLAB Synergy Dualflex diffractometer with a HyPix detector	Huber 4-circle
Absorption correction	Multi-scan (*CrysAlis PRO*; Rigaku OD, 2023)	Multi-scan (*SADABS*; Bruker, 2018)
T_{min}, T_{max}	0.807, 1.000	0.853, 1.000
No. of measured, independent and observed [$I > 2\sigma(I)$] reflections	29802, 5815, 5188	44621, 9816, 9201
R_{int}	0.035	0.048
$(\sin\theta/\lambda)_{max}$ (Å^{-1})	0.723	0.881
Refinement		
$R[F^2 > 2\sigma(F^2)]$, $wR(F^2)$, S	0.032, 0.080, 1.05	0.032, 0.084, 1.09
No. of reflections	5815	9816
No. of parameters	437	419
No. of restraints	340	66
$\Delta\rho_{max}$, $\Delta\rho_{min}$ (e Å^{-3})	0.71, −0.49	0.42, −0.87

Computer programs: *CrysAlis PRO* (Rigaku OD, 2023), *APEX3* (Bruker, 2018), *SAINT* (Bruker, 2018), *SHELXT2018* (Sheldrick, 2015*a*), *SHELXL2019* (Sheldrick, 2015*b*), and *OLEX2* (Dolomanov *et al.*, 2009).

et al., 2020) complexes. We typically obtain $Fe(hfac)_3$ by the procedure described by Morris *et al.* (1963) with two important modifications: (i) using CH_2Cl_2 instead of CCl_4 as a solvent medium and (ii) purifying the bulk product by sublimation at 44 °C or by recrystallization from the melt at 55 °C. Despite the fact that we have successfully applied 'as-synthesized' crystalline/microcrystalline $Fe(hfac)_3$ in several synthetic procedures, its powder X-ray diffraction (PXRD) pattern appears as notably different from that calculated from the only reported structural data in the Cambridge Structural Database [CSD (Groom *et al.*, 2016) refcode BUPTAH ($P2_1/c$; deposition No. CCDC 1117036; Pfluger & Haradem, 1983)] (Fig. 1). Based on the search, the $M(hfac)_3$ structures deposited in the CSD appear either as monoclinic or trigonal/hexagonal. Among those structures, only $Cr(hfac)_3$ and $Rh(hfac)_3$ feature both monoclinic ($P2_1/n$) and trigonal ($P\overline{3}c1$)/hexagonal ($P6/mmm$) modifications (Jessop *et al.*, 2002; Harada & Girolami, 2007; Davignon *et al.*, 1970). Other metal diketonates are reported as either monoclinic $P2_1/n$ [V (Calderazzo *et al.*, 2005), Mn (Bouwman *et al.*, 1993), Ga (Ballarin *et al.*, 1994), and Ru (Baird *et al.*, 1999)] or trigonal/hexagonal $P\overline{3}c1$ (Al; Bouyahyi *et al.*, 2010), $P\overline{3}$ (Mo; Champouret *et al.*, 2010), and $P6/mmm$ (Ir; Davignon *et al.*, 1970). Some of the trivalent metals, notably $Co(hfac)_3$, lack any reported structural data. While the PXRD pattern of our 'as-synthesized' $Fe(hfac)_3$ does not match with that reported in the CSD (monoclinic space group), it appears very similar to the powder pattern of $Cr(hfac)_3$ calculated for its trigonal modification (Fig. 1). Herein, we report the trigonal modification of $Fe(hfac)_3$ and recollect the crystal structure of its monoclinic form, while changing the space-group assignment based on the high-quality data collected. The former can be

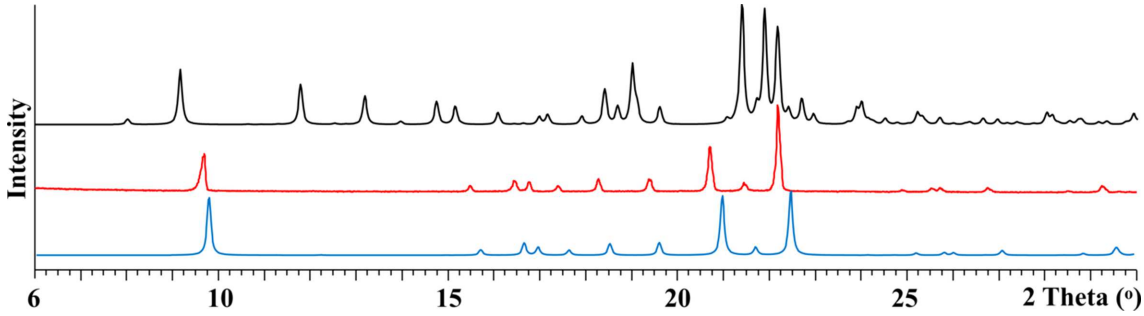

Figure 1
Powder X-ray pattern comparison: calculated pattern of the monoclinic $Fe(hfac)_3$ reported in the CSD (black); experimental pattern of 'as synthesized' in this work $Fe(hfac)_3$ (red); calculated pattern of trigonal $Cr(hfac)_3$ (blue).

regarded as a 'high-temperature' polymorph, while the latter represents a 'low-temperature' modification. A comparison is also made of the physical properties and characterization of these two forms.

2. Experimental

All of the manipulations were carried out in a dry oxygen-free argon atmosphere by employing standard Schlenk and glove-box techniques. Anhydrous iron(III) chloride ($FeCl_3$) and hexafluoroacetylacetone (Hhfac) were purchased from Sigma–Aldrich and used as received. Dichloromethane (DCM) was purchased from Sigma–Aldrich and was dried and degassed before use. Powder X-ray diffraction data were collected on a Rigaku multipurpose θ–θ X-ray SmartLab SE diffractometer [Cu $K\alpha$ radiation, HyPix-400 two-dimensional advanced photo-counting hybrid pixel array detector (Rigaku, Tokyo, Japan), with a step of 0.01° 2θ at 20 °C]. Le Bail fit refinement for the powder diffraction patterns was performed using the *TOPAS 4* software package (Bruker, 2006). The DSC spectra were recorded on a DSC 2500 differential calorimeter (TA instrument, New Castle, DE, USA). The DART-MS spectra were acquired on an AccuTof 4G LC-plus DART mass spectrometer (JEOL, Tokyo, Japan). The IR spectra were measured using an IRTracer-100 Fourier Transform Infrared spectrophotometer (Shimadzu, Kyoto, Japan). The melting-point temperatures were determined using a Stuart SMP11/120V/60 melting point apparatus (Bibby Sterilin, Staffordshire, UK).

2.1. Synthesis and crystallization

2.1.1. Preparation of the low-temperature modification of Fe(hfac)$_3$ (1-L). A flask was charged with anhydrous $FeCl_3$ (1.00 g, 6.2 mmol) under a dry argon atmosphere, and dry oxygen-free DCM (20 ml) was added. Upon stirring, Hhfac (3.00 ml, 21.19 mmol) was added to the solution. The dark-red solution was stirred for 24 h. The reaction mixture was filtered, and the filtrate was evaporated and dried under vacuum at room temperature to obtain a powdered solid. Crystals were grown by sealing the microcrystalline powder in an evacuated glass ampule placed above a sand bath with a temperature of 26 °C. The ampule had a temperature gradient (*ca* 5 °C) along the length of the tube and was kept at this temperature for 3 d, allowing crystals of **1-L** to appear in the cold section of the container where the temperature was *ca* 21 °C. Crystals of **1-L** can also be grown by the slow evaporation of a hexanes solution in open air.

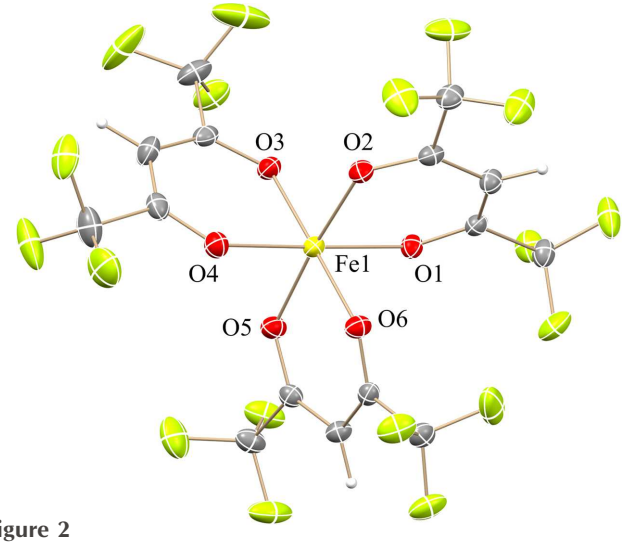

Figure 2
The atom-numbering scheme for the **1-L** modification of Fe(hfac)$_3$, with displacement ellipsoids drawn at the 50% probability level. H atoms are shown as spheres of arbitrary radius. Only one orientation of the disordered CF_3 groups is depicted.

Table 2
Selected bond lengths and angles (Å, °) for **1-L** and **1-H**.

	1-L		**1-H**
Fe1—O1	1.9899 (11)	Fe1—O1	1.9914 (8)
Fe1—O2	2.0045 (11)	Fe1—O2	2.0070 (8)
Fe1—O3	1.9921 (11)	Fe2—O3	1.9866 (8)
Fe1—O4	1.9891 (11)	Fe2—O4	1.9997 (8)
Fe1—O5	1.9939 (11)	Fe3—O5	1.9948 (9)
Fe1—O6	1.9971 (11)	Fe3—O6	2.0012 (9)
O1—Fe1—O2	87.36 (4)	O1—Fe1—O1^{i}	92.74 (3)
O1—Fe1—O3	92.08 (5)	O1—Fe1—O2	86.68 (3)
O1—Fe1—O4	178.59 (5)	O1—Fe1—O2^{i}	92.17 (3)
O1—Fe1—O5	90.33 (5)	O1—Fe1—O2^{ii}	175.07 (3)
O1—Fe1—O6	87.96 (5)	O2—Fe1—O2^{i}	88.45 (4)
O2—Fe1—O3	92.11 (5)	O3—Fe2—O3^{iii}	92.73 (3)
O2—Fe1—O4	91.33 (5)	O3—Fe2—O4	87.36 (4)
O2—Fe1—O5	175.27 (4)	O4—Fe2—O3^{iii}	90.95 (4)
O2—Fe1—O6	88.60 (5)	O4—Fe2—O3^{iv}	176.31 (4)
O3—Fe1—O4	87.45 (5)	O4—Fe2—O4^{iii}	88.95 (4)
O3—Fe1—O5	92.08 (4)	O5—Fe3—O5^{v}	92.30 (3)
O3—Fe1—O6	179.29 (5)	O5—Fe3—O6	87.01 (4)
O4—Fe1—O5	91.02 (5)	O5—Fe3—O6^{v}	176.66 (4)
O4—Fe1—O6	92.53 (5)	O5—Fe3—O6^{vi}	90.99 (4)
O5—Fe1—O6	87.20 (4)	O6—Fe3—O6^{v}	89.74 (4)

Symmetry codes: (i) $-x+y+1, -x+2, z$; (ii) $-y+2, x-y+1, z$; (iii) $-y+1, x-y, z$; (iv) $-x+y+1, -x+1, z$; (v) $-y+1, x-y+1, z$; (vi) $-x+y, -x+1, z$.

2.1.2. Preparation of the high-temperature modification of Fe(hfac)$_3$ (1-H). The microcrystalline powder of **1-L** was sealed in an evacuated glass ampule and placed in a furnace having a temperature gradient along the length of the tube. The ampule was kept at 55 °C for 7 d to allow the crystals of **1-H** to recrystallize from the melt upon slow cooling to room temperature. Crystals of **1-H** can also be obtained by keeping the ampule in a gradient furnace at 44 °C to allow the compound to sublime and deposit in the cold zone of the container, where the temperature was set at 41 °C.

2.2. Refinement

Crystal data, data collection, and structure refinement details for both **1-L** and **1-H** are summarized in Table 1, and the selected metric parameters are given in Table 2. The atom-numbering schemes for **1-L** and **1-H** are shown in Figs. 2 and 3, respectively. For both structures, the H atoms were included in the model at geometrically calculated positions and refined using a riding model. The isotropic displacement parameters of all H atoms were fixed at 1.2 times the U_{eq} value of the

atoms to which they were linked. In the structures of **1-L** and **1-H**, one and two CF_3 groups, respectively, were found to be disordered. All disordered CF_3 groups were modeled with two (in **1-H**) or three (in **1-L**) orientations, with their relative occupancies refined. The geometries of the disordered parts were restrained to be similar. The anisotropic displacement parameters of all disordered groups were restrained to have the same U_{ij} components, with a standard uncertainty of 0.01 Å^2. The structure of **1-H** was refined as a two-component merohedral twin, with the relative batch scale factor (BASF) converging to 0.2097 (6).

3. Results and discussion

$Fe(hfac)_3$ is a mononuclear molecule, in which the iron center is chelated by three hfac ligands. The structure has been solved and refined in the monoclinic space group $P2_1/n$ for **1-L** (Fig. 2) and in the trigonal space group $P\overline{3}$ for **1-H** (Fig. 3). It should be noted that **1-L** was refined in the space group $P2_1/n$ rather than $P2_1/c$ in a previous report (Pfluger & Haradem, 1983) as a commonly accepted standard setting with a closer to 90° β-angle value. Both modifications are centrosymmetric and feature an equal number of Λ- and Δ-enantiomeric forms (Scheme 1). The average Fe—O bond lengths in **1-L** and **1-H** are 1.9944 (11) and 1.9967 (8) Å, respectively. The bond lengths determined in the present work are similar to those reported previously, *i.e.* 1.999 (10) Å. The O—Fe—O bond angles in **1-L** and **1-H** are in the range 86.68 (3)–92.74 (3)°, which are close to the values obtained earlier (Pfluger & Haradem, 1983).

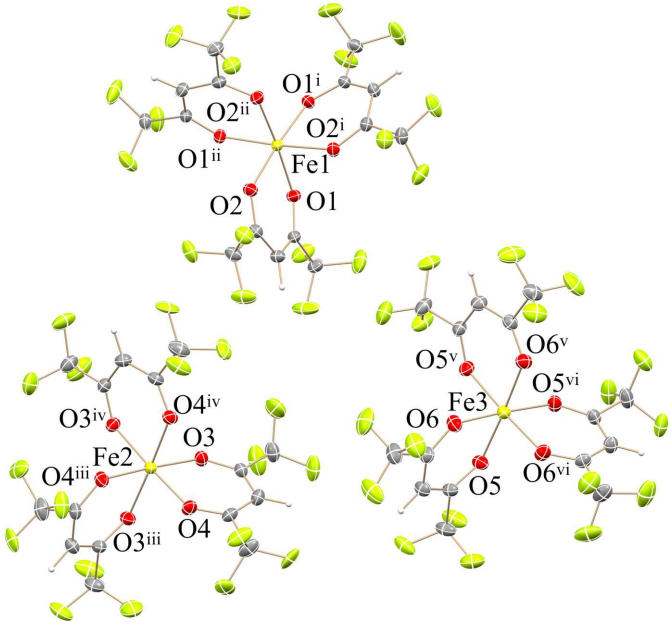

Figure 3
The atom-numbering scheme for the **1-H** modification of $Fe(hfac)_3$, with displacement ellipsoids drawn at the 50% probability level. H atoms are shown as spheres of arbitrary radius. Only one orientation of the disordered CF_3 groups is depicted. [Symmetry codes: (i) $-x+y+1, -x+2, z$; (ii) $-y+2, x-y+1, z$; (iii) $-y+1, x-y, z$; (iv) $-x+y+1, -x+1, z$; (v) $-y+1, x-y+1, z$; (vi) $-x+y, -x+1, z$.]

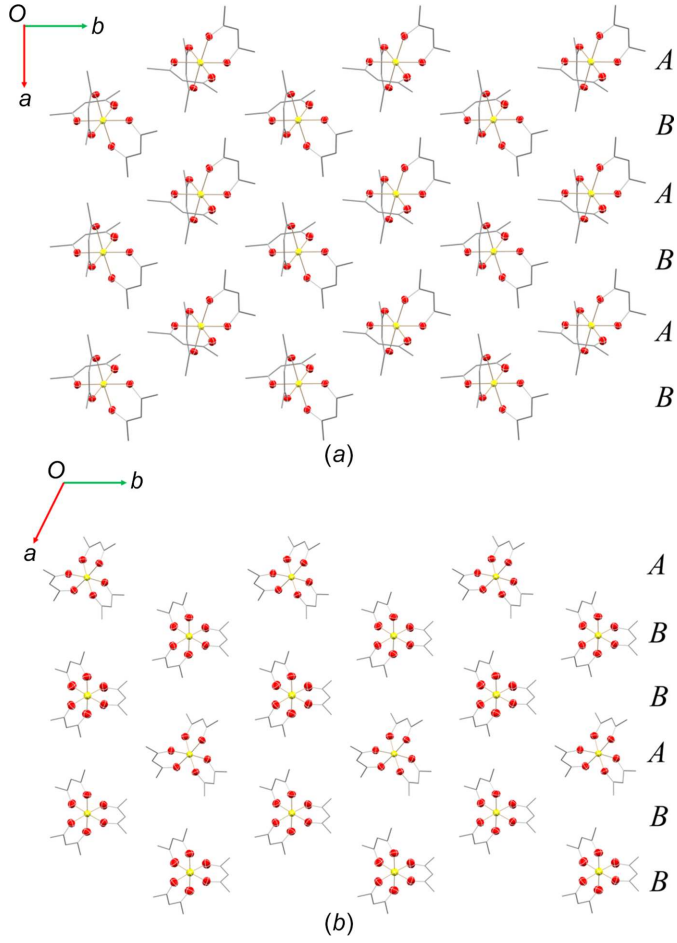

Figure 4
Packing diagrams along the *c* axis for (*a*) **1-L** and (*b*) **1-H**, rendered as space-filling models for the $[FeO_6]$ core, as well as capped sticks models for C atoms. Only Fe, O, and C atoms are shown for clarity. Colour scheme used: Fe yellow, O red, and C grey.

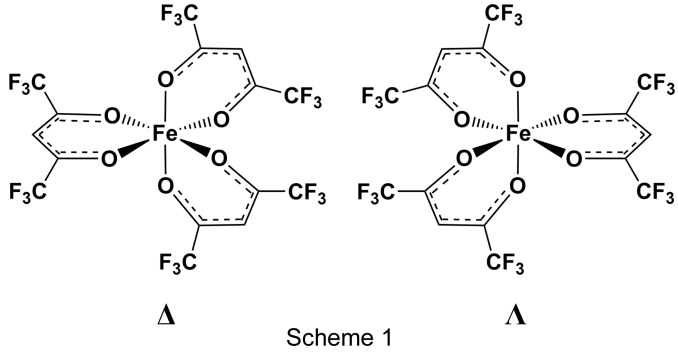

Scheme 1

1-L and **1-H** are two polymorph modifications of $Fe(hfac)_3$ that are packed in a different way. The packing diagram of **1-L** [Fig. 4(*a*)] shows that the $[Fe(hfac)_3]$ molecules are arranged in an *ABAB* manner, while in **1-H**, the packing order is *ABBABB* [Fig. 4(*b*)].

Despite **1-L** and **1-H** experiencing a different mutual arrangement of *tris*-chelated Fe molecules, most of the physical properties of these polymorphs are similar. They are

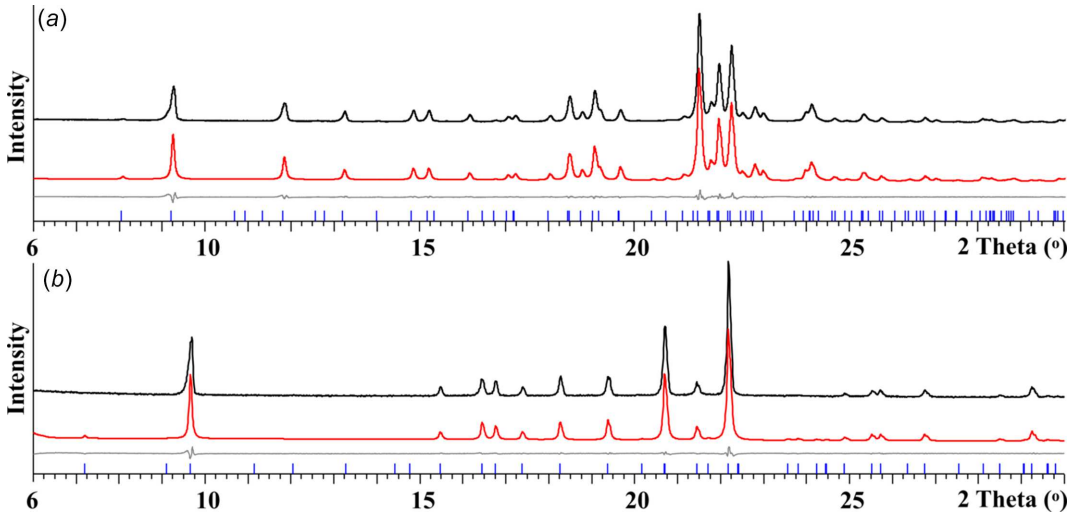

Figure 5
Powder X-ray diffraction patterns of the (*a*) **1-L** and (*b*) **1-H** bulk products and the Le Bail fits. Black and red curves represent experimental and calculated patterns, respectively. Gray is the difference curve with theoretical peak positions shown as blue bars at the bottom.

both soluble in most common organic solvents, such as hexanes, toluene, tetrahydrofuran (THF), acetone, and alcohols. They are quite sensitive to moisture, which is indicated by a color change from dark red to yellow when exposed to open air for less than 30 min. However, the melting points of **1-L** and **1-H** are different, being recorded as 50 and 46 °C, respectively, when measured in sealed capillary tubes. $Fe(hfac)_3$ was found to decompose in a sealed evacuated glass ampule at around 280 °C. The phase purity of the bulk products has been investigated by powder X-ray diffraction (PXRD). The PXRD pattern of $Fe(hfac)_3$ prepared in solution at room temperature corresponds to the monoclinic modification **1-L** [Fig. 5(*a*)] according to the Le Bail fit. A crystalline sample obtained upon crystallization of **1-L** from the melt at 55 °C shows a PXRD pattern [Fig. 5(*b*)] that matches the theoretical pattern calculated from the single-crystal X-ray data of the trigonal **1-H** polymorph.

Fig. 6 shows the differential scanning calorimetry (DSC) analysis of **1-L** and **1-H** between 20 and 60 °C, with a scanning rate of 0.5 °C min^{-1}. In both **1-L** and **1-H** plots, only one endothermic and one exothermic peak were registered during the heating and cooling processes, respectively, in all cycles. The curve for solid **1-L** [Fig. 6(*a*)] features during the first cycle an endothermic peak at 53.0 °C, which corresponds to its

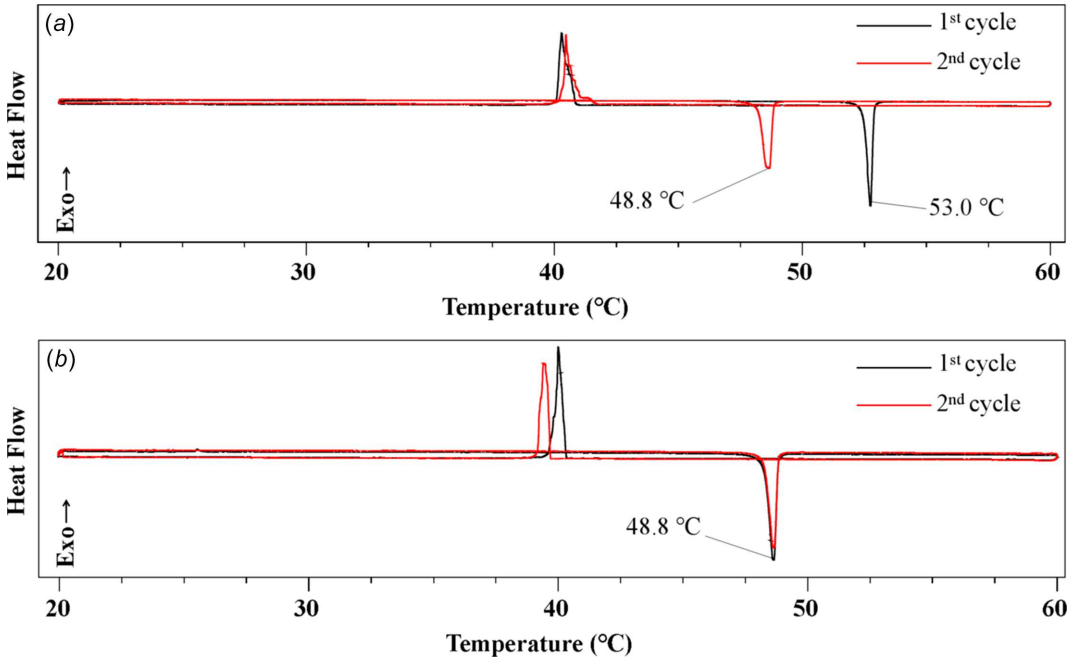

Figure 6
DSC analysis of (*a*) **1-L** and (*b*) **1-H**, with a heating rate of 0.5 °C min^{-1}. Black and red curves represent the first and second cycle, respectively. The following cycles (not shown) are identical to the second one.

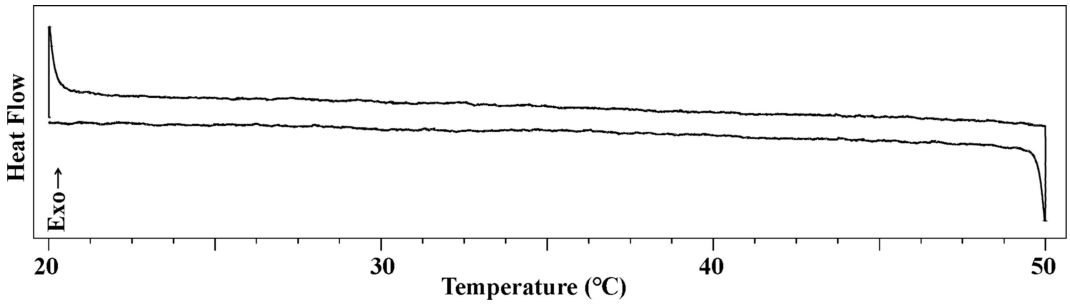

Figure 7
DSC analysis of **1-L** between 20 and 50 °C, with a heating rate of 0.5 °C min^{-1}.

melting point. An exothermic peak, also known as the crystallization temperature (or the freezing point), appears at about 40 °C upon cooling. Beginning with the second cycle, the endothermic peak is shifted to 48.8 °C, corresponding to the melting point of **1-H**, that also crystallizes at around 40 °C. The residue collected after the DSC measurements was confirmed to be the high-temperature modification of Fe(hfac)$_3$ by powder X-ray diffraction. On the other hand, in the measurements of **1-H** [Fig. 6(*b*)], the endothermic peak (melting point) was recorded at 48.8 °C upon heating, and the exothermic peak (freezing point) was observed at around 39–40 °C on a cooling process in every cycle. The heat hysteresis between the melting and freezing points is obviously due to the effect of supercooling (Menczel *et al.*, 2009). It is important that the DSC results fully support our previous observations of the different melting points of **1-L** and **1-H** as 50 and 46 °C, respectively, in sealed capillary tubes.

The possibility of transformation from low- to high-temperature modifications of Fe(hfac)$_3$ in the solid state was also tested by DSC analysis. The measurements of **1-L** (Fig. 7) confirmed that there is no endothermic or exothermic signals between 20 and 50 °C, below its melting point. In addition, the powder of **1-L** was sealed in an evacuated ampule and placed in a nongradient furnace at 45 °C. After several days of annealing, the PXRD pattern confirmed the presence of only the low-temperature modification. These results indicate the absence of a phase transformation between **1-L** and **1-H** in the solid state (crystal-to-crystal).

All observations clearly demonstrate that **1-L** can be transformed to **1-H** only upon crystallization from the melt at around 40 °C or by crystallization from the gas phase at 44/41 °C. At the same time, the low-temperature modification of Fe(hfac)$_3$ can be isolated by sublimation at 26/21 °C or by crystallization from solution at room or lower temperatures.

The positive-mode direct analysis in real-time mass spectrometry (DART-MS) of the solid Fe(hfac)$_3$ features the $[Fe(hfac)_2]^+$ ion $\{[M(hfac)]^+\}$ with a characteristic isotope distribution pattern. The measured/calculated (m/z) values are

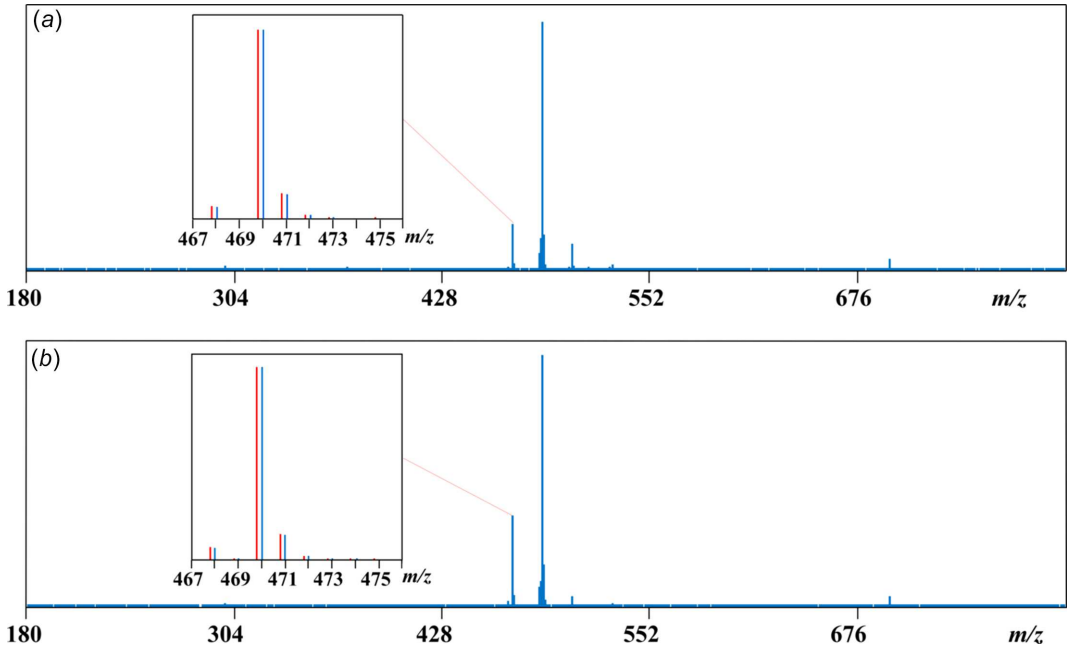

Figure 8
Positive-ion DART mass spectrum of solid (*a*) **1-L** and (*b*) **1-H** measured at 300 °C. The isotope distribution patterns for the $[Fe(hfac)_2]^+$ ion are shown in the insets. Blue and red lines are experimental and calculated patterns, respectively.

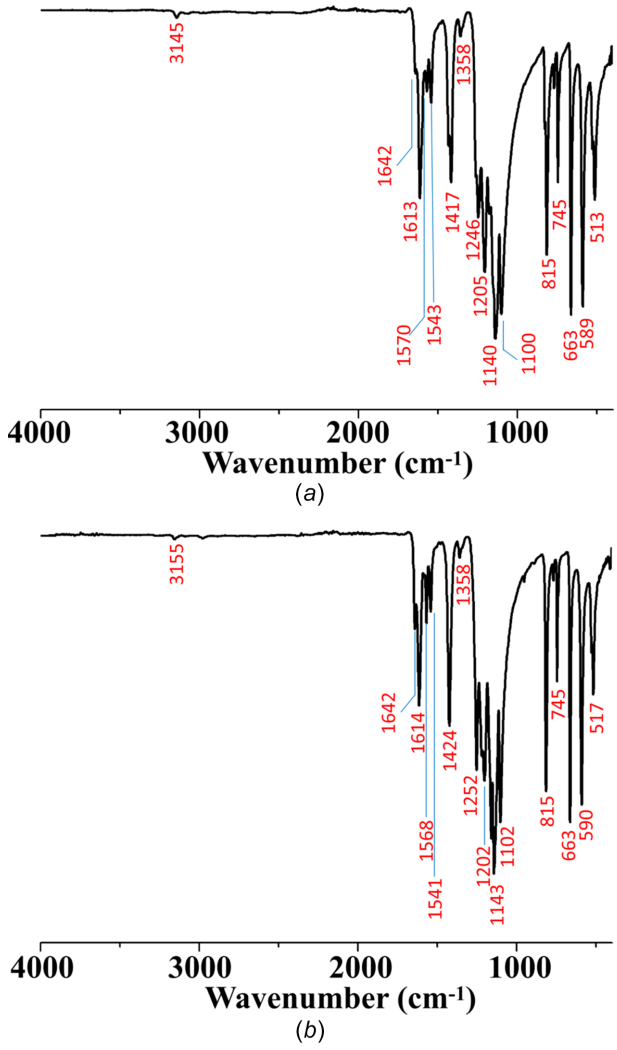

Figure 9
The attenuated total reflection (ATR) spectra of (*a*) **1-L** and (*b*) **1-H**.

469.9241/469.9110 and 469.9065/469.9110 for **1-L** and **1-H**, respectively (Fig. 8). Two modifications cannot be recognized by mass spectrometry; the assignments of fragment ions are listed in Table 3.

The attenuated total reflection (ATR) spectra of **1-L** and **1-H** (Fig. 9) are almost identical. Both spectra show some typical peaks like the C═O, C═C, C—F, and C—C stretching at 1613, 1641, 1252, and 663 cm^{-1}, respectively, which were also listed in a previous report (Morris *et al.*, 1963).

Table 3
Assignment of ions detected in the positive-mode DART-MS spectra of **1-L** and **1-H** (hfac = $C_5HF_6O_2$).

Ions	Measured, *m*/*z*	Calculated, *m*/*z*	Δ	% Base
1-L				
$[Fe(hfac)_2]^+$	469.9241	469.9110	0.0131	18.51
$[Fe(hfac)_2{\cdot}H_2O]^+$	487.9358	487.9216	0.0142	100.00
$[Fe(hfac)_2{\cdot}2H_2O]^+$	505.9463	505.9322	0.0141	10.66
$[Fe(hfac)_3{\cdot}NH_4]^+$	694.9616	694.9335	0.0281	4.64
1-H				
$[Fe(hfac)_2]^+$	469.9065	469.9110	0.0045	35.96
$[Fe(hfac)_2{\cdot}H_2O]^+$	487.9194	487.9216	0.0022	100.00
$[Fe(hfac)_2{\cdot}2H_2O]^+$	505.9279	505.9322	0.0043	4.03
$[Fe(hfac)_3{\cdot}NH_4]^+$	694.9329	694.9335	0.0006	4.07

4. Conclusions

Iron(III) hexafluoroacetylacetonate was established to have two polymorph modifications, namely, the monoclinic low-temperature and the trigonal high-temperature form. The discovery of the $Fe(hfac)_3$ trigonal modification resolves the long-standing issue that the PXRD pattern of bulk $Fe(hfac)_3$ obtained by purification at 44–55 °C does not correspond to that calculated form the reported crystal data. Other trivalent transition-metal $M(hfac)_3$ complexes, such as the Mn and Co ones, have been obtained in a similar way and used in the synthesis by us (Zhang, Li, Sun *et al.*, 2008; Zhang, Li & Dikarev, 2008; Zhang *et al.*, 2009; Lieberman *et al.*, 2017). However, both $Mn(hfac)_3$ and $Co(hfac)_3$ also face a similar problem that their PXRD patterns either do not match that reported in the CSD (Mn) or have no entries to compare with (Co). Although the syntheses of bulk $Mn(hfac)_3$ and $Co(hfac)_3$ have been established for a very long time, their high-temperature modifications (as well as the low-temperature modification of Co) are not supported by X-ray diffraction data, since suitable single crystals appear hard to grow and solve (Zhang, Li, Sun *et al.*, 2008). At the same time, it is evident that the PXRD patterns of trivalent Mn and Co hexafluoroacetylacetonates look very similar to that of the high-temperature modification of $Fe(hfac)_3$ (Fig. 10). It now seems likely that other trivalent metal (V, Ga, and Ru) hexafluoroacetylacetonates also appear as low- and high-

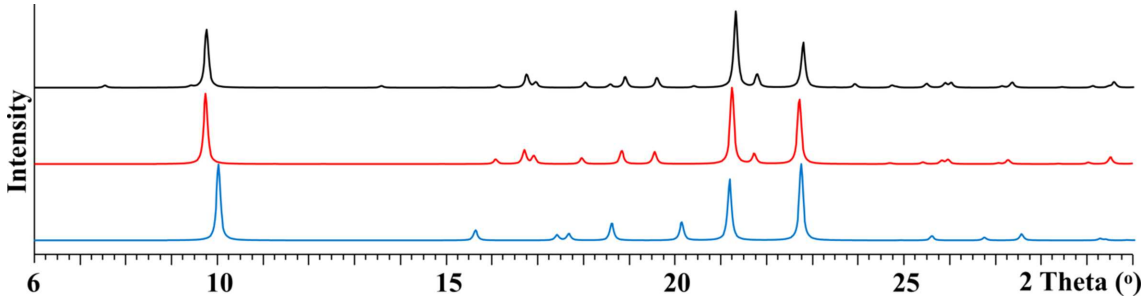

Figure 10
Comparison of the powder X-ray diffraction patterns of $Fe(hfac)_3$ (black), $Mn(hfac)_3$ (red), and $Co(hfac)_3$ (blue) obtained upon sublimation.

temperature polymorphs. Therefore, this investigation of two modifications of $Fe(hfac)_3$ may help to avoid the misidentification of this broad family of complexes that are very important starting reagents in various synthetic procedures.

Acknowledgements

Financial support from the National Science Foundation is gratefully acknowledged. NSF's ChemMatCARS, Sector 15 at the Advanced Photon Source (APS), Argonne National Laboratory (ANL), is supported by the Divisions of Chemistry (CHE) and Materials Research (DMR), National Science Foundation. This research used resources of the Advanced Photon Source, a US Department of Energy (DOE) Office of Science user facility operated for the DOE Office of Science by Argonne National Laboratory under contract No. DE-AC02-06CH11357. The structure of **1-L** was solved and refined by undergraduate student Julianna N. Defeo as her final project in the Crystallography course (CHM 470) in the fall semester of 2022.

Funding information

Funding for this research was provided by: the National Science Foundation (grant Nos. CHE-1955585 and CHE-2400091 to Evgeny V. Dikarev; grant No. CHE-1834750 to Matthew Tirrell).

References

Baird, I. R., Rettig, S. J., James, B. R. & Skov, K. A. (1999). *Can. J. Chem.* **77**, 1821–1833.

Ballarin, B., Battiston, G. A., Benetollo, F., Gerbasi, R., Porchia, M., Favretto, D. & Traldi, P. (1994). *Inorg. Chim. Acta*, **217**, 71–78.

Barry, M. C., Lieberman, C. M., Wei, Z., Clérac, R., Filatov, A. S. & Dikarev, E. V. (2018). *Inorg. Chem.* **57**, 2308–2313.

Battiston, G. A., Gerbasi, R., Porchia, M., Bertoncello, R. & Caccavale, F. (1996). *Thin Solid Films*, **279**, 115–118.

Bespalova, P. G., Vorobyev, A. A., Kunkel, T. S., Shakhmin, A. L. & Mishin, M. V. (2020). *Mater. Today Proc.* **30**, 434–438.

Bouwman, E., Caulton, K. G., Christou, G., Folting, K., Gasser, C., Hendrickson, D. N., Huffman, J. C., Lobkovsky, E. B. & Martin, J. D. (1993). *Inorg. Chem.* **32**, 3463–3470.

Bouyahyi, M., Roisnel, T. & Carpentier, J.-F. (2010). *Organometallics*, **29**, 491–500.

Bruker (2006). *TOPAS 4*. Bruker AXS Inc., Madison, Wisconsin, USA.

Bruker (2018). *APEX3*, *SADABS*, and *SAINT*. Bruker AXS Inc., Madison, Wisconsin, USA.

Bryant, J. R., Taves, J. E. & Mayer, J. M. (2002). *Inorg. Chem.* **41**, 2769–2776.

Calderazzo, F., Englert, U., Pampaloni, G. & Volpe, M. (2005). *J. Organomet. Chem.* **690**, 3321–3332.

Chakravarty, B. & Adhikari, S. (1991). *Transition Met. Chem.* **16**, 586–591.

Champouret, Y., Poli, R. & Daran, J.-C. (2010). *Acta Cryst.* E**66**, m299–m300.

Chokprasombat, K., Harding, P., Sirisathitkul, C., Tangwatanakul, W., Pinitsoontorn, S. & Muneesawang, P. (2014). *J. Nanopart. Res.* **16**, 1–8.

Conradie, J. (2022). *J. Electrochem. Soc.* **169**, 046522.

Conradie, M. M. & Conradie, J. (2015). *Electrochim. Acta*, **152**, 512–519.

Crowder, J. M., Han, H., Wei, Z., Dikarev, E. V. & Petrukhina, M. A. (2019). *Polyhedron*, **157**, 33–38.

Davignon, L., Manoli, J. M. & Dereigne, A. (1970). *J. Less-Common Met.* **21**, 341–344.

Denmark, S. E. & Cresswell, A. J. (2013). *J. Org. Chem.* **78**, 12593–12628.

Dhar, S., Arod, P., Achari, K. V. L. V. N. & Shivashankar, S. A. (2015). *MRS Online Proceedings Library*, **1752**, 45–50.

Dolomanov, O. V., Bourhis, L. J., Gildea, R. J., Howard, J. A. K. & Puschmann, H. (2009). *J. Appl. Cryst.* **42**, 339–341.

Drath, O., Gable, R. W., Moubaraki, B., Murray, K. S. & Boskovic, C. (2018). *Polyhedron*, **151**, 323–329.

Fahlman, B. D. & Barron, A. R. (2000). *Adv. Mater. Opt. Electron.* **10**, 223–232.

Freitag, R. & Conradie, J. (2015). *Electrochim. Acta*, **158**, 418–426.

Gostynski, R., Conradie, J. & Erasmus, E. (2017). *RSC Adv.* **7**, 27718–27728.

Gostynski, R., Conradie, M. M., Liu, R. Y. & Conradie, J. (2016). *JNanoR*, **44**, 252–264.

Groom, C. R., Bruno, I. J., Lightfoot, M. P. & Ward, S. C. (2016). *Acta Cryst.* B**72**, 171–179.

Han, H., Carozza, J. C., Colliton, A. P., Zhang, Y., Wei, Z., Filatov, A. S., Chen, Y.-S., Alkan, M., Rogachev, A. Yu. & Dikarev, E. V. (2020). *Angew. Chem. Int. Ed.* **59**, 9624–9630.

Harada, Y. & Girolami, G. S. (2007). *Polyhedron*, **26**, 1758–1762.

Jessop, P. G., Olmstead, M. M., Ablan, C. D., Grabenauer, M., Sheppard, D., Eckert, C. A. & Liotta, C. L. (2002). *Inorg. Chem.* **41**, 3463–3468.

Kato, K. & Mukaiyama, T. (1992). *Chem. Lett.* **21**, 1137–1140.

Lassègue, P., Noé, L., Monthioux, M. & Caussat, B. (2015). *Phys. Status Solidi (C)*, **12**, 861–868.

Lee, F.-J., Chi, Y., Liu, C.-S., Hsu, P.-F., Chou, T.-Y., Peng, S.-M. & Lee, G.-H. (2001). *Chem. Vap. Depos.* **7**, 99–101.

Lieberman, C. M., Barry, M. C., Wei, Z., Rogachev, A. Yu., Wang, X., Liu, J.-L., Clérac, R., Chen, Y.-S., Filatov, A. S. & Dikarev, E. V. (2017). *Inorg. Chem.* **56**, 9574–9584.

Lieberman, C. M., Filatov, A., Wei, Z., Rogachev, A. Yu., Abakumov, A. M. & Dikarev, E. V. (2015). *Chem. Sci.* **6**, 2835–2842.

Ma, Y., Reardon, D., Gambarotta, S., Yap, G., Zahalka, H. & Lemay, C. (1999). *Organometallics*, **18**, 2773–2781.

Makhaev, V. D. & Petrova, L. A. (2017). *Russ. J. Gen. Chem.* **87**, 1105–1109.

Menczel, J. D., Judovits, L., Prime, R. B., Bair, H. E., Reading, M. & Swier, S. (2009). *Thermal Analysis of Polymers: Fundamentals and Applications*, edited by J. D. Menczel & R. B. Prime, pp. 7–239. Hoboken: John Wiley & Sons, Inc.

Mishra, S. & Daniele, S. (2015). *Chem. Rev.* **115**, 8379–8448.

Morris, M. L., Moshier, R. W. & Sievers, R. E. (1963). *Inorg. Chem.* **2**, 411–412.

Moxon, N. T., Moffett, J. H. & Gregson, A. K. (1981). *J. Inorg. Nucl. Chem.* **43**, 2695–2702.

Navulla, A., Tsirlin, A. A., Abakumov, A. M., Shpanchenko, R. V., Zhang, H. & Dikarev, E. V. (2011). *J. Am. Chem. Soc.* **133**, 692–694.

Neumann, S. M. & Kochi, J. K. (1975). *J. Org. Chem.* **40**, 599–606.

Opwis, K., Plohl, D., Schneider, J., Seithuemmer, J., Wunschik, D. S. & Gutmann, J. S. (2022). *J. Supercrit. Fluids*, **191**, 105722.

Peng, Q., Hojo, D., Park, K. J. & Parsons, G. N. (2008). *Thin Solid Films*, **516**, 4997–5003.

Pfluger, C. E. & Haradem, P. S. (1983). *Inorg. Chim. Acta*, **69**, 141–146.

Rigaku OD (2023). *CrysAlis PRO*. Rigaku Oxford Diffraction Ltd, Yarnton, Oxfordshire, England.

Sheldrick, G. M. (2015*a*). *Acta Cryst.* A**71**, 3–8.

Sheldrick, G. M. (2015*b*). *Acta Cryst.* C**71**, 3–8.

Sievers, R. E. & Sadlowski, J. E. (1978). *Science*, **201**, 217–223.

Smolentsev, A. I., Zherikova, K. V., Trusov, M. S., Stabnikov, P. A., Naumov, D. Yu. & Borisov, S. V. (2011). *J. Struct. Chem.* **52**, 1070–1077.

Stienen, C. & Bendt, G. (2020). *ChemSusChem*, **13**, 5954–5961.
Takai, T., Hata, E., Yamada, T. & Mukaiyama, T. (1991). *Bull. Chem. Soc. Jpn*, **64**, 2513–2518.
Talaga, D. S., Hanna, S. D. & Zink, J. I. (1998). *Inorg. Chem.* **37**, 2880–2887.
Tangwatanakul, W., Chokprasombat, K., Sirisathitkul, C., Jantaratana, P. & Sirisathitkul, Y. (2016). *J. Alloys Compd.* **654**, 234–239.
Umecky, T., Kanakubo, M. & Ikushima, Y. (2011). *J. Phys. Chem. B*, **115**, 10622–10630.
Waidmann, C. R., Miller, A. J. M., Ng, C. A., Scheuermann, M. L., Porter, T. R., Tronic, T. A. & Mayer, J. M. (2012). *Energy Environ. Sci.* **5**, 7771–7780.
Wei, Z., Filatov, A. S. & Dikarev, E. V. (2013). *J. Am. Chem. Soc.* **135**, 12216–12219.
Woo, C. M., Gholap, S. L., Lu, L., Kaneko, M., Li, Z., Ravikumar, P. C. & Herzon, S. B. (2012). *J. Am. Chem. Soc.* **134**, 17262–17273.
Zhang, H., Li, B. & Dikarev, E. V. (2008). *J. Cluster Sci.* **19**, 311–321.
Zhang, H., Li, B., Sun, J., Clérac, R. & Dikarev, E. V. (2008). *Inorg. Chem.* **47**, 10046–10052.
Zhang, H., Yang, J.-H., Shpanchenko, R. V., Abakumov, A. M., Hadermann, J., Clérac, R. & Dikarev, E. V. (2009). *Inorg. Chem.* **48**, 8480–8488.
Zherikova, K. V., Zelenina, L. N., Chusova, T. P., Morozova, N. B., Trubin, S. V. & Vikulova, E. S. (2013). *Phys. Procedia*, **46**, 200–208.

supporting information

Acta Cryst. (2024). C**80**, 567-575 [https://doi.org/10.1107/S2053229624007575]

Two polymorph modifications of tris(hexafluoroacetylacetonato)iron(III) revealed: is that common for other trivalent metals?

Joyce Chang, Julianna N. Defeo, Zheng Wei and Evgeny V. Dikarev

Computing details

Tris(1,1,1,5,5,5-hexafluoro-4-oxopent-2-en-2-olato)iron(III) (1-L)

Crystal data

$[Fe(C_5HF_6O_2)_3]$
M_r = 677.02
Monoclinic, $P2_1/n$
a = 8.7659 (2) Å
b = 12.9796 (3) Å
c = 19.1759 (5) Å
β = 91.632 (2)°
V = 2180.90 (9) Å^3
Z = 4
$F(000)$ = 1316
D_x = 2.062 Mg m^{-3}
Mo $K\alpha$ radiation, λ = 0.71073 Å
Cell parameters from 21755 reflections
θ = 1.9–31.1°
μ = 0.88 mm^{-1}
T = 100 K
Block, red
0.16 × 0.12 × 0.09 mm

Data collection

Rigaku XtaLAB Synergy Dualflex diffractometer with a HyPix detector
Radiation source: micro-focus sealed X-ray tube
Mirror monochromator
Detector resolution: 10.0000 pixels mm^{-1}
ω scans
Absorption correction: multi-scan (CrysAlis PRO; Rigaku OD, 2023)
T_{min} = 0.807, T_{max} = 1.000
29802 measured reflections
5815 independent reflections
5188 reflections with $I > 2\sigma(I)$
R_{int} = 0.035
θ_{max} = 30.9°, θ_{min} = 1.9°
h = −12→12
k = −18→18
l = −26→21

Refinement

Refinement on F^2
Least-squares matrix: full
$R[F^2 > 2\sigma(F^2)]$ = 0.032
$wR(F^2)$ = 0.080
S = 1.05
5815 reflections
437 parameters
340 restraints
Primary atom site location: dual
Secondary atom site location: difference Fourier map
Hydrogen site location: inferred from neighbouring sites
H-atom parameters constrained
$w = 1/[\sigma^2(F_o^2) + (0.0337P)^2 + 1.5613P]$ where $P = (F_o^2 + 2F_c^2)/3$
$(\Delta/\sigma)_{max}$ = 0.001
$\Delta\rho_{max}$ = 0.71 e Å^{-3}
$\Delta\rho_{min}$ = −0.49 e Å^{-3}
Extinction correction: SHELXL2019 (Sheldrick, 2015b), $Fc^*=kFc[1+0.001xFc^2\lambda^3/\sin(2\theta)]^{-1/4}$
Extinction coefficient: 0.0015 (2)

Special details

Geometry. All esds (except the esd in the dihedral angle between two l.s. planes) are estimated using the full covariance matrix. The cell esds are taken into account individually in the estimation of esds in distances, angles and torsion angles; correlations between esds in cell parameters are only used when they are defined by crystal symmetry. An approximate (isotropic) treatment of cell esds is used for estimating esds involving l.s. planes.

Fractional atomic coordinates and isotropic or equivalent isotropic displacement parameters (Å²)

	x	*y*	*z*	U_{iso}*/U_{eq}	Occ. (<1)
Fe1	0.46900 (2)	0.49202 (2)	0.72339 (2)	0.01693 (7)	
O1	0.57997 (12)	0.55097 (8)	0.80610 (5)	0.0185 (2)	
O2	0.27477 (12)	0.52851 (9)	0.77026 (6)	0.0204 (2)	
O3	0.47272 (12)	0.62615 (8)	0.67298 (6)	0.0199 (2)	
O4	0.35357 (13)	0.43511 (9)	0.64130 (6)	0.0231 (2)	
O5	0.66633 (12)	0.44825 (8)	0.68348 (6)	0.0206 (2)	
O6	0.46767 (12)	0.35703 (8)	0.77335 (6)	0.0208 (2)	
C1	0.64970 (18)	0.57904 (13)	0.92318 (8)	0.0227 (3)	
C2	0.52614 (17)	0.56446 (11)	0.86604 (8)	0.0173 (3)	
C3	0.37466 (17)	0.56599 (12)	0.88408 (8)	0.0203 (3)	
H3	0.348842	0.576705	0.931306	0.024*	
C4	0.25941 (17)	0.55187 (11)	0.83328 (8)	0.0189 (3)	
C5	0.09413 (18)	0.57213 (13)	0.85443 (9)	0.0242 (3)	
C6	0.4270 (2)	0.76326 (14)	0.59627 (10)	0.0305 (4)	
C7	0.41157 (17)	0.64876 (12)	0.61483 (8)	0.0200 (3)	
C8	0.3346 (2)	0.58291 (14)	0.56906 (8)	0.0266 (3)	
H8	0.294569	0.608734	0.525938	0.032*	
C9	0.31523 (18)	0.47960 (13)	0.58556 (8)	0.0228 (3)	
C11	0.89668 (18)	0.36581 (12)	0.66105 (9)	0.0236 (3)	
C12	0.74973 (17)	0.37331 (11)	0.70213 (8)	0.0183 (3)	
C13	0.71970 (17)	0.29929 (11)	0.75225 (8)	0.0200 (3)	
H13	0.795415	0.249771	0.764805	0.024*	
C14	0.57945 (17)	0.29747 (11)	0.78402 (7)	0.0172 (3)	
C15	0.54919 (18)	0.21521 (12)	0.83934 (8)	0.0224 (3)	
F1	0.75797 (11)	0.64274 (8)	0.90242 (5)	0.0283 (2)	
F2	0.71521 (13)	0.48824 (9)	0.93766 (6)	0.0362 (3)	
F3	0.59418 (12)	0.61549 (11)	0.98224 (5)	0.0388 (3)	
F4	0.06344 (13)	0.67176 (9)	0.84624 (7)	0.0430 (3)	
F5	0.07236 (12)	0.54738 (11)	0.92035 (6)	0.0395 (3)	
F6	−0.00539 (12)	0.51973 (11)	0.81544 (7)	0.0427 (3)	
F7	0.34009 (17)	0.81936 (9)	0.63729 (9)	0.0629 (4)	
F8	0.38449 (18)	0.78312 (11)	0.53107 (8)	0.0616 (4)	
F9	0.56915 (12)	0.79520 (8)	0.60523 (6)	0.0346 (2)	
F13	0.86086 (13)	0.35067 (10)	0.59334 (6)	0.0416 (3)	
F14	0.97807 (11)	0.45122 (8)	0.66567 (6)	0.0326 (2)	
F15	0.98408 (13)	0.28783 (8)	0.68154 (7)	0.0399 (3)	
F16	0.66232 (12)	0.14777 (8)	0.84594 (6)	0.0328 (2)	
F17	0.53208 (17)	0.25995 (9)	0.90105 (5)	0.0442 (3)	
F18	0.42170 (11)	0.16378 (8)	0.82345 (6)	0.0324 (2)	

C10	0.237 (4)	0.410 (2)	0.5286 (13)	0.0315 (18)	0.395 (3)
F10	0.2012 (14)	0.3222 (13)	0.5514 (7)	0.047 (2)	0.395 (3)
F11	0.0996 (6)	0.4562 (7)	0.5074 (4)	0.0420 (14)	0.395 (3)
F12	0.3186 (7)	0.4093 (6)	0.4738 (3)	0.0524 (16)	0.395 (3)
C10X	0.268 (2)	0.405 (2)	0.5270 (13)	0.036 (2)	0.263 (3)
F10X	0.1355 (8)	0.3686 (7)	0.5421 (4)	0.0576 (18)	0.263 (3)
F11X	0.2545 (11)	0.4523 (5)	0.4649 (3)	0.0505 (17)	0.263 (3)
F12X	0.3659 (9)	0.3294 (5)	0.5210 (3)	0.0386 (14)	0.263 (3)
C10Y	0.240 (4)	0.407 (3)	0.5329 (14)	0.034 (2)	0.342 (3)
F10Y	0.1750 (16)	0.3215 (14)	0.5617 (8)	0.0313 (16)	0.342 (3)
F11Y	0.1430 (10)	0.4470 (7)	0.4898 (4)	0.054 (2)	0.342 (3)
F12Y	0.3533 (7)	0.3629 (6)	0.4936 (4)	0.0454 (18)	0.342 (3)

Atomic displacement parameters (Å²)

	U^{11}	U^{22}	U^{33}	U^{12}	U^{13}	U^{23}
Fe1	0.01857 (11)	0.01664 (11)	0.01548 (11)	0.00176 (8)	−0.00116 (8)	0.00129 (8)
O1	0.0159 (5)	0.0235 (5)	0.0162 (5)	0.0004 (4)	0.0001 (4)	0.0000 (4)
O2	0.0170 (5)	0.0234 (5)	0.0205 (5)	0.0030 (4)	−0.0020 (4)	0.0004 (4)
O3	0.0227 (5)	0.0181 (5)	0.0186 (5)	0.0012 (4)	−0.0027 (4)	0.0015 (4)
O4	0.0261 (6)	0.0223 (5)	0.0206 (5)	−0.0010 (4)	−0.0025 (4)	−0.0030 (4)
O5	0.0227 (5)	0.0182 (5)	0.0212 (5)	0.0023 (4)	0.0037 (4)	0.0029 (4)
O6	0.0202 (5)	0.0195 (5)	0.0228 (5)	0.0016 (4)	0.0019 (4)	0.0037 (4)
C1	0.0186 (7)	0.0317 (8)	0.0177 (7)	−0.0013 (6)	−0.0016 (6)	−0.0007 (6)
C2	0.0182 (7)	0.0168 (6)	0.0168 (6)	0.0003 (5)	−0.0018 (5)	0.0022 (5)
C3	0.0185 (7)	0.0252 (7)	0.0171 (7)	0.0006 (6)	0.0013 (6)	0.0021 (6)
C4	0.0166 (7)	0.0179 (7)	0.0222 (7)	0.0018 (5)	0.0007 (6)	0.0041 (6)
C5	0.0171 (7)	0.0298 (8)	0.0257 (8)	0.0030 (6)	0.0002 (6)	0.0027 (6)
C6	0.0268 (8)	0.0275 (8)	0.0370 (9)	0.0027 (7)	−0.0036 (7)	0.0130 (7)
C7	0.0164 (7)	0.0228 (7)	0.0209 (7)	0.0053 (5)	0.0020 (6)	0.0041 (6)
C8	0.0273 (8)	0.0340 (9)	0.0182 (7)	0.0007 (7)	−0.0054 (6)	0.0043 (7)
C9	0.0186 (7)	0.0314 (8)	0.0184 (7)	0.0009 (6)	0.0013 (6)	−0.0053 (6)
C11	0.0238 (8)	0.0178 (7)	0.0297 (8)	−0.0009 (6)	0.0069 (6)	−0.0006 (6)
C12	0.0188 (7)	0.0162 (6)	0.0198 (7)	−0.0011 (5)	0.0007 (5)	−0.0025 (5)
C13	0.0195 (7)	0.0173 (7)	0.0230 (7)	0.0006 (5)	−0.0005 (6)	0.0022 (6)
C14	0.0210 (7)	0.0142 (6)	0.0163 (6)	−0.0024 (5)	−0.0021 (5)	0.0000 (5)
C15	0.0263 (8)	0.0181 (7)	0.0227 (7)	−0.0006 (6)	0.0016 (6)	0.0045 (6)
F1	0.0192 (4)	0.0371 (6)	0.0283 (5)	−0.0070 (4)	−0.0025 (4)	−0.0038 (4)
F2	0.0330 (6)	0.0399 (6)	0.0348 (6)	0.0050 (5)	−0.0133 (5)	0.0109 (5)
F3	0.0255 (5)	0.0712 (8)	0.0197 (5)	−0.0047 (5)	0.0003 (4)	−0.0132 (5)
F4	0.0281 (5)	0.0334 (6)	0.0681 (8)	0.0142 (5)	0.0124 (5)	0.0098 (6)
F5	0.0215 (5)	0.0688 (8)	0.0285 (5)	0.0060 (5)	0.0074 (4)	0.0115 (5)
F6	0.0166 (5)	0.0646 (8)	0.0467 (7)	−0.0055 (5)	−0.0002 (5)	−0.0150 (6)
F7	0.0587 (8)	0.0234 (6)	0.1087 (13)	0.0136 (6)	0.0372 (9)	0.0086 (7)
F8	0.0736 (10)	0.0517 (8)	0.0574 (8)	−0.0152 (7)	−0.0357 (7)	0.0360 (7)
F9	0.0308 (5)	0.0285 (5)	0.0441 (6)	−0.0053 (4)	−0.0054 (5)	0.0125 (5)
F13	0.0390 (6)	0.0579 (8)	0.0285 (6)	−0.0093 (5)	0.0130 (5)	−0.0098 (5)
F14	0.0229 (5)	0.0208 (5)	0.0546 (7)	−0.0055 (4)	0.0088 (5)	−0.0041 (5)

F15	0.0326 (6)	0.0283 (5)	0.0599 (8)	0.0129 (4)	0.0203 (5)	0.0133 (5)
F16	0.0278 (5)	0.0264 (5)	0.0441 (6)	0.0030 (4)	−0.0004 (4)	0.0174 (5)
F17	0.0808 (9)	0.0331 (6)	0.0192 (5)	−0.0007 (6)	0.0093 (5)	0.0035 (4)
F18	0.0242 (5)	0.0256 (5)	0.0476 (6)	−0.0067 (4)	0.0026 (4)	0.0120 (5)
C10	0.030 (4)	0.047 (3)	0.018 (3)	−0.014 (3)	−0.002 (3)	−0.016 (3)
F10	0.059 (6)	0.041 (3)	0.040 (5)	−0.014 (4)	−0.012 (3)	−0.010 (3)
F11	0.0237 (19)	0.067 (3)	0.034 (3)	−0.0147 (19)	−0.0100 (15)	0.001 (2)
F12	0.037 (3)	0.092 (5)	0.029 (3)	−0.022 (3)	0.012 (2)	−0.032 (3)
C10X	0.035 (4)	0.045 (4)	0.027 (4)	−0.004 (4)	−0.001 (4)	−0.009 (3)
F10X	0.039 (3)	0.085 (5)	0.049 (4)	−0.029 (3)	0.011 (3)	−0.036 (3)
F11X	0.074 (5)	0.055 (3)	0.021 (2)	0.001 (3)	−0.018 (3)	−0.010 (2)
F12X	0.054 (3)	0.035 (3)	0.027 (3)	0.005 (2)	0.001 (3)	−0.017 (2)
C10Y	0.029 (4)	0.050 (4)	0.023 (4)	−0.008 (3)	0.009 (3)	−0.002 (3)
F10Y	0.030 (3)	0.035 (3)	0.029 (3)	−0.016 (2)	0.007 (2)	−0.009 (2)
F11Y	0.069 (5)	0.050 (3)	0.040 (4)	−0.003 (4)	−0.033 (3)	−0.008 (3)
F12Y	0.034 (3)	0.064 (5)	0.039 (4)	−0.013 (3)	0.022 (3)	−0.030 (3)

Geometric parameters (Å, º)

Fe1—O1	1.9899 (11)	C7—C8	1.387 (2)
Fe1—O2	2.0045 (11)	C8—H8	0.9500
Fe1—O3	1.9921 (11)	C8—C9	1.389 (2)
Fe1—O4	1.9891 (11)	C9—C10	1.563 (9)
Fe1—O5	1.9939 (11)	C9—C10X	1.532 (13)
Fe1—O6	1.9971 (11)	C9—C10Y	1.518 (12)
O1—C2	1.2670 (18)	C11—C12	1.532 (2)
O2—C4	1.2568 (19)	C11—F13	1.342 (2)
O3—C7	1.2582 (18)	C11—F14	1.3199 (18)
O4—C9	1.252 (2)	C11—F15	1.3224 (19)
O5—C12	1.2624 (18)	C12—C13	1.389 (2)
O6—C14	1.2603 (18)	C13—H13	0.9500
C1—C2	1.530 (2)	C13—C14	1.388 (2)
C1—F1	1.3283 (19)	C14—C15	1.534 (2)
C1—F2	1.337 (2)	C15—F16	1.3261 (19)
C1—F3	1.3321 (19)	C15—F17	1.3303 (19)
C2—C3	1.382 (2)	C15—F18	1.3297 (19)
C3—H3	0.9500	C10—F10	1.26 (3)
C3—C4	1.395 (2)	C10—F11	1.39 (3)
C4—C5	1.538 (2)	C10—F12	1.29 (4)
C5—F4	1.329 (2)	C10X—F10X	1.29 (2)
C5—F5	1.3233 (19)	C10X—F11X	1.34 (3)
C5—F6	1.321 (2)	C10X—F12X	1.31 (2)
C6—C7	1.535 (2)	C10Y—F10Y	1.37 (3)
C6—F7	1.328 (2)	C10Y—F11Y	1.28 (4)
C6—F8	1.320 (2)	C10Y—F12Y	1.39 (4)
C6—F9	1.319 (2)		
O1—Fe1—O2	87.36 (4)	C8—C7—C6	119.65 (15)

O1—Fe1—O3	92.08 (4)	C7—C8—H8	119.6
O1—Fe1—O5	90.33 (5)	C7—C8—C9	120.74 (15)
O1—Fe1—O6	87.96 (5)	C9—C8—H8	119.6
O3—Fe1—O2	92.11 (5)	O4—C9—C8	127.44 (15)
O3—Fe1—O5	92.08 (4)	O4—C9—C10	115.6 (11)
O3—Fe1—O6	179.29 (5)	O4—C9—C10X	113.2 (13)
O4—Fe1—O1	178.59 (5)	O4—C9—C10Y	112.5 (14)
O4—Fe1—O2	91.33 (5)	C8—C9—C10	117.0 (11)
O4—Fe1—O3	87.45 (5)	C8—C9—C10X	118.5 (12)
O4—Fe1—O5	91.02 (5)	C8—C9—C10Y	120.0 (14)
O4—Fe1—O6	92.53 (5)	F13—C11—C12	109.26 (13)
O5—Fe1—O2	175.27 (4)	F14—C11—C12	111.89 (13)
O5—Fe1—O6	87.20 (4)	F14—C11—F13	107.40 (14)
O6—Fe1—O2	88.60 (5)	F14—C11—F15	108.39 (14)
C2—O1—Fe1	126.15 (10)	F15—C11—C12	112.61 (13)
C4—O2—Fe1	127.14 (10)	F15—C11—F13	107.05 (14)
C7—O3—Fe1	128.42 (10)	O5—C12—C11	113.08 (13)
C9—O4—Fe1	128.49 (11)	O5—C12—C13	127.53 (14)
C12—O5—Fe1	127.77 (10)	C13—C12—C11	119.36 (13)
C14—O6—Fe1	126.94 (10)	C12—C13—H13	119.9
F1—C1—C2	111.07 (13)	C14—C13—C12	120.21 (14)
F1—C1—F2	107.74 (13)	C14—C13—H13	119.9
F1—C1—F3	108.38 (14)	O6—C14—C13	127.78 (14)
F2—C1—C2	109.31 (13)	O6—C14—C15	112.98 (13)
F3—C1—C2	112.60 (13)	C13—C14—C15	119.24 (13)
F3—C1—F2	107.56 (13)	F16—C15—C14	112.46 (13)
O1—C2—C1	113.10 (13)	F16—C15—F17	107.83 (14)
O1—C2—C3	127.91 (14)	F16—C15—F18	108.17 (13)
C3—C2—C1	118.99 (13)	F17—C15—C14	109.72 (13)
C2—C3—H3	119.8	F18—C15—C14	110.60 (13)
C2—C3—C4	120.35 (14)	F18—C15—F17	107.92 (14)
C4—C3—H3	119.8	F10—C10—C9	112.8 (18)
O2—C4—C3	127.42 (14)	F10—C10—F11	106 (2)
O2—C4—C5	114.98 (13)	F10—C10—F12	115 (2)
C3—C4—C5	117.52 (14)	F11—C10—C9	108.2 (18)
F4—C5—C4	108.92 (13)	F12—C10—C9	109.2 (19)
F5—C5—C4	111.89 (13)	F12—C10—F11	105.1 (18)
F5—C5—F4	108.35 (15)	F10X—C10X—C9	107.1 (13)
F6—C5—C4	111.99 (14)	F10X—C10X—F11X	108.2 (17)
F6—C5—F4	107.81 (14)	F10X—C10X—F12X	110 (2)
F6—C5—F5	107.74 (14)	F11X—C10X—C9	112.0 (18)
F7—C6—C7	109.72 (14)	F12X—C10X—C9	111.8 (15)
F8—C6—C7	112.59 (16)	F12X—C10X—F11X	107.7 (15)
F8—C6—F7	107.60 (16)	F10Y—C10Y—C9	114 (2)
F9—C6—C7	111.31 (13)	F10Y—C10Y—F12Y	101 (2)
F9—C6—F7	107.83 (17)	F11Y—C10Y—C9	117 (3)
F9—C6—F8	107.60 (15)	F11Y—C10Y—F10Y	108 (2)
O3—C7—C6	113.14 (14)	F11Y—C10Y—F12Y	106.8 (19)

O3—C7—C8	127.21 (15)	F12Y—C10Y—C9	108 (2)
Fe1—O1—C2—C1	162.11 (10)	C6—C7—C8—C9	−178.15 (15)
Fe1—O1—C2—C3	−17.1 (2)	C7—C8—C9—O4	4.1 (3)
Fe1—O2—C4—C3	5.6 (2)	C7—C8—C9—C10	−176.0 (16)
Fe1—O2—C4—C5	−177.78 (10)	C7—C8—C9—C10X	−164.4 (8)
Fe1—O3—C7—C6	174.55 (10)	C7—C8—C9—C10Y	−176.1 (19)
Fe1—O3—C7—C8	−4.8 (2)	C8—C9—C10—F10	−169.1 (19)
Fe1—O4—C9—C8	−5.1 (2)	C8—C9—C10—F11	−53 (2)
Fe1—O4—C9—C10	175.0 (16)	C8—C9—C10—F12	61 (2)
Fe1—O4—C9—C10X	163.9 (8)	C8—C9—C10X—F10X	−116.8 (18)
Fe1—O4—C9—C10Y	175.1 (17)	C8—C9—C10X—F11X	1.6 (17)
Fe1—O5—C12—C11	−177.80 (10)	C8—C9—C10X—F12X	122.6 (18)
Fe1—O5—C12—C13	4.3 (2)	C8—C9—C10Y—F10Y	−156 (2)
Fe1—O6—C14—C13	−14.7 (2)	C8—C9—C10Y—F11Y	−28 (4)
Fe1—O6—C14—C15	165.23 (10)	C8—C9—C10Y—F12Y	92 (2)
O1—C2—C3—C4	−0.2 (3)	C11—C12—C13—C14	−172.25 (14)
O2—C4—C5—F4	−90.73 (17)	C12—C13—C14—O6	0.1 (2)
O2—C4—C5—F5	149.50 (14)	C12—C13—C14—C15	−179.82 (14)
O2—C4—C5—F6	28.4 (2)	C13—C14—C15—F16	−5.4 (2)
O3—C7—C8—C9	1.2 (3)	C13—C14—C15—F17	114.61 (16)
O4—C9—C10—F10	11 (3)	C13—C14—C15—F18	−126.46 (15)
O4—C9—C10—F11	127.4 (15)	F1—C1—C2—O1	44.26 (18)
O4—C9—C10—F12	−118.7 (17)	F1—C1—C2—C3	−136.47 (15)
O4—C9—C10X—F10X	73.1 (19)	F2—C1—C2—O1	−74.49 (16)
O4—C9—C10X—F11X	−168.4 (11)	F2—C1—C2—C3	104.77 (16)
O4—C9—C10X—F12X	−47 (2)	F3—C1—C2—O1	166.02 (14)
O4—C9—C10Y—F10Y	23 (4)	F3—C1—C2—C3	−14.7 (2)
O4—C9—C10Y—F11Y	151 (2)	F7—C6—C7—O3	−70.26 (19)
O4—C9—C10Y—F12Y	−88 (2)	F7—C6—C7—C8	109.16 (19)
O5—C12—C13—C14	5.6 (2)	F8—C6—C7—O3	169.94 (15)
O6—C14—C15—F16	174.67 (13)	F8—C6—C7—C8	−10.6 (2)
O6—C14—C15—F17	−65.31 (17)	F9—C6—C7—O3	49.0 (2)
O6—C14—C15—F18	53.62 (18)	F9—C6—C7—C8	−131.56 (17)
C1—C2—C3—C4	−179.35 (14)	F13—C11—C12—O5	−61.96 (17)
C2—C3—C4—O2	6.4 (3)	F13—C11—C12—C13	116.16 (16)
C2—C3—C4—C5	−170.13 (14)	F14—C11—C12—O5	56.85 (18)
C3—C4—C5—F4	86.24 (17)	F14—C11—C12—C13	−125.03 (16)
C3—C4—C5—F5	−33.5 (2)	F15—C11—C12—O5	179.23 (14)
C3—C4—C5—F6	−154.61 (15)	F15—C11—C12—C13	−2.7 (2)

Tris(1,1,1,5,5,5-hexafluoro-4-oxopent-2-en-2-olato)iron(III) (1-H)

Crystal data

$[Fe(C_5HF_6O_2)_3]$	c = 11.7136 (3) Å
M_r = 677.02	V = 3328.54 (17) Å^3
Trigonal, $P\overline{3}$	Z = 6
a = 18.1141 (4) Å	$F(000)$ = 1974

D_x = 2.026 Mg m^{-3}
Synchrotron radiation, λ = 0.41329 Å
Cell parameters from 9909 reflections
θ = 2.4–21.1°
μ = 0.21 mm^{-1}
T = 100 K
Block, red
0.15 × 0.12 × 0.09 mm

Data collection

Huber 4-circle diffractometer
Radiation source: synchrotron
Si(111) & Si(311) monochromator
Detector resolution: 30 pixels mm^{-1}
φ scans
Absorption correction: multi-scan (SADABS; Bruker, 2018)
T_{min} = 0.853, T_{max} = 1.000
44621 measured reflections
9816 independent reflections
9201 reflections with $I > 2\sigma(I)$
R_{int} = 0.048
θ_{max} = 21.4°, θ_{min} = 1.0°
h = −24→25
k = −25→31
l = −17→20

Refinement

Refinement on F^2
Least-squares matrix: full
$R[F^2 > 2\sigma(F^2)]$ = 0.032
$wR(F^2)$ = 0.084
S = 1.09
9816 reflections
419 parameters
66 restraints
Primary atom site location: dual
Secondary atom site location: difference Fourier map
Hydrogen site location: inferred from neighbouring sites
H-atom parameters constrained
$w = 1/[\sigma^2(F_o^2) + (0.0325P)^2 + 0.8379P]$ where $P = (F_o^2 + 2F_c^2)/3$
$(\Delta/\sigma)_{max}$ = 0.002
$\Delta\rho_{max}$ = 0.42 e Å^{-3}
$\Delta\rho_{min}$ = −0.87 e Å^{-3}
Extinction correction: SHELXL2019 (Sheldrick, 2015b), $Fc^*=kFc[1+0.001xFc^2\lambda^3/\sin(2\theta)]^{-1/4}$
Extinction coefficient: 0.0612 (18)

Special details

Geometry. All esds (except the esd in the dihedral angle between two l.s. planes) are estimated using the full covariance matrix. The cell esds are taken into account individually in the estimation of esds in distances, angles and torsion angles; correlations between esds in cell parameters are only used when they are defined by crystal symmetry. An approximate (isotropic) treatment of cell esds is used for estimating esds involving l.s. planes.
Refinement. Refined as a 2-component twin.

Fractional atomic coordinates and isotropic or equivalent isotropic displacement parameters (Å^2)

	x	y	z	U_{iso}*/U_{eq}	Occ. (<1)
Fe1	1.000000	1.000000	0.71400 (2)	0.01654 (5)	
Fe2	0.666667	0.333333	0.51162 (2)	0.01865 (5)	
Fe3	0.333333	0.666667	0.93886 (2)	0.02110 (6)	
O1	0.89940 (5)	0.92050 (5)	0.62066 (7)	0.01976 (14)	
O2	0.97128 (5)	0.89995 (5)	0.81556 (7)	0.02078 (14)	
O3	0.61280 (6)	0.38529 (6)	0.41847 (7)	0.02248 (14)	
O4	0.56364 (5)	0.28567 (6)	0.61197 (7)	0.02412 (15)	
O5	0.28244 (6)	0.56081 (5)	0.84457 (7)	0.02463 (15)	
O6	0.38193 (7)	0.61141 (7)	1.03795 (7)	0.02682 (16)	
C1	0.76554 (7)	0.80956 (8)	0.56148 (10)	0.02247 (19)	
C2	0.83980 (7)	0.84721 (7)	0.64728 (9)	0.01791 (16)	
C3	0.83466 (7)	0.79900 (7)	0.74320 (9)	0.02029 (18)	

H3	0.784606	0.745835	0.757020	0.024*	
C4	0.90328 (7)	0.82924 (7)	0.81852 (8)	0.01883 (17)	
C5	0.90137 (8)	0.77069 (7)	0.91514 (9)	0.0236 (2)	
C6	0.53188 (10)	0.44576 (10)	0.35758 (11)	0.0300 (3)	
C7	0.54744 (7)	0.39018 (7)	0.44150 (9)	0.01997 (18)	
C8	0.49062 (8)	0.35176 (8)	0.53137 (9)	0.02246 (19)	
H8	0.443465	0.360613	0.540069	0.027*	
C9	0.50280 (7)	0.30028 (8)	0.60868 (9)	0.02141 (19)	
C12	0.28010 (8)	0.49139 (7)	0.86520 (9)	0.02183 (19)	
C13	0.32037 (8)	0.47359 (8)	0.95365 (9)	0.0242 (2)	
H13	0.314621	0.418651	0.959664	0.029*	
C14	0.36896 (8)	0.53643 (8)	1.03300 (9)	0.02281 (19)	
C15	0.41563 (10)	0.51552 (11)	1.12642 (11)	0.0325 (3)	
F1	0.79368 (6)	0.82446 (7)	0.45473 (7)	0.0376 (2)	
F2	0.71822 (7)	0.84609 (8)	0.57490 (9)	0.0427 (2)	
F3	0.71500 (7)	0.72637 (6)	0.57427 (10)	0.0483 (3)	
F4	0.95881 (7)	0.74648 (6)	0.89470 (7)	0.03534 (19)	
F5	0.82540 (6)	0.70044 (6)	0.92495 (8)	0.0385 (2)	
F6	0.92051 (6)	0.81077 (5)	1.01509 (6)	0.02827 (16)	
F7	0.59348 (8)	0.52668 (7)	0.36801 (12)	0.0514 (3)	
F8	0.53281 (9)	0.42204 (9)	0.25058 (7)	0.0491 (3)	
F9	0.45868 (7)	0.44381 (8)	0.37561 (8)	0.0422 (2)	
F16	0.49857 (7)	0.55425 (10)	1.10301 (10)	0.0514 (3)	
F17	0.38688 (9)	0.43233 (7)	1.13467 (9)	0.0509 (3)	
F18	0.40698 (8)	0.54366 (7)	1.22734 (7)	0.0415 (2)	
C10	0.43433 (9)	0.25160 (11)	0.69967 (11)	0.0335 (3)	
F10	0.3909 (6)	0.1711 (4)	0.6730 (6)	0.0654 (14)	0.75 (3)
F11	0.3809 (6)	0.2822 (9)	0.7073 (7)	0.0672 (17)	0.75 (3)
F12	0.4692 (5)	0.2603 (5)	0.8012 (4)	0.0390 (11)	0.75 (3)
F10X	0.4049 (10)	0.1657 (7)	0.6835 (17)	0.043 (3)	0.25 (3)
F11X	0.3675 (7)	0.2612 (10)	0.6983 (16)	0.038 (2)	0.25 (3)
F12X	0.4670 (12)	0.2644 (15)	0.8049 (12)	0.039 (4)	0.25 (3)
C11	0.22338 (9)	0.41848 (8)	0.78326 (11)	0.0308 (3)	
F13	0.1407 (5)	0.3902 (10)	0.8150 (7)	0.062 (2)	0.53 (5)
F14	0.2364 (11)	0.3541 (7)	0.7912 (14)	0.054 (2)	0.53 (5)
F15	0.2347 (11)	0.4497 (8)	0.6776 (5)	0.0340 (13)	0.53 (5)
F13X	0.1446 (5)	0.3774 (7)	0.8169 (5)	0.0414 (16)	0.47 (5)
F14X	0.2486 (7)	0.3602 (7)	0.7731 (10)	0.0356 (14)	0.47 (5)
F15X	0.2222 (15)	0.4436 (10)	0.6786 (8)	0.042 (3)	0.47 (5)

Atomic displacement parameters (Å²)

	U^{11}	U^{22}	U^{33}	U^{12}	U^{13}	U^{23}
Fe1	0.01379 (7)	0.01379 (7)	0.02205 (10)	0.00689 (3)	0.000	0.000
Fe2	0.01576 (7)	0.01576 (7)	0.02441 (11)	0.00788 (4)	0.000	0.000
Fe3	0.01905 (8)	0.01905 (8)	0.02521 (11)	0.00952 (4)	0.000	0.000
O1	0.0163 (3)	0.0171 (3)	0.0237 (3)	0.0067 (3)	−0.0016 (3)	0.0021 (3)
O2	0.0197 (3)	0.0170 (3)	0.0244 (3)	0.0083 (3)	−0.0033 (3)	0.0008 (3)

O3	0.0225 (4)	0.0228 (4)	0.0256 (3)	0.0139 (3)	0.0047 (3)	0.0057 (3)
O4	0.0190 (3)	0.0243 (4)	0.0276 (3)	0.0098 (3)	0.0030 (3)	0.0083 (3)
O5	0.0252 (4)	0.0197 (3)	0.0273 (3)	0.0099 (3)	−0.0077 (3)	−0.0006 (3)
O6	0.0285 (4)	0.0268 (4)	0.0286 (3)	0.0164 (3)	−0.0097 (3)	−0.0062 (3)
C1	0.0162 (4)	0.0232 (5)	0.0239 (4)	0.0068 (4)	−0.0021 (3)	0.0015 (4)
C2	0.0155 (4)	0.0166 (4)	0.0208 (4)	0.0074 (3)	−0.0014 (3)	−0.0013 (3)
C3	0.0193 (4)	0.0165 (4)	0.0213 (4)	0.0061 (4)	−0.0005 (3)	0.0011 (3)
C4	0.0218 (5)	0.0166 (4)	0.0189 (3)	0.0102 (4)	0.0000 (3)	−0.0003 (3)
C5	0.0299 (6)	0.0186 (4)	0.0205 (4)	0.0107 (4)	−0.0023 (4)	0.0006 (3)
C6	0.0377 (7)	0.0363 (7)	0.0274 (5)	0.0271 (6)	0.0029 (4)	0.0064 (5)
C7	0.0222 (5)	0.0202 (4)	0.0200 (4)	0.0125 (4)	−0.0010 (3)	−0.0002 (3)
C8	0.0197 (5)	0.0292 (5)	0.0211 (4)	0.0143 (4)	−0.0001 (3)	−0.0009 (4)
C9	0.0159 (4)	0.0245 (5)	0.0194 (4)	0.0068 (4)	0.0008 (3)	0.0010 (3)
C12	0.0215 (5)	0.0188 (4)	0.0213 (4)	0.0071 (4)	−0.0027 (3)	0.0008 (3)
C13	0.0291 (6)	0.0221 (5)	0.0218 (4)	0.0132 (4)	−0.0034 (4)	0.0014 (4)
C14	0.0229 (5)	0.0281 (5)	0.0205 (4)	0.0151 (4)	−0.0032 (3)	−0.0006 (4)
C15	0.0395 (7)	0.0412 (7)	0.0270 (5)	0.0278 (6)	−0.0127 (5)	−0.0073 (5)
F1	0.0264 (4)	0.0510 (6)	0.0214 (3)	0.0088 (4)	−0.0025 (3)	−0.0056 (3)
F2	0.0311 (4)	0.0616 (7)	0.0485 (5)	0.0330 (5)	−0.0119 (4)	−0.0118 (5)
F3	0.0373 (5)	0.0248 (4)	0.0562 (6)	−0.0044 (4)	−0.0257 (4)	0.0084 (4)
F4	0.0544 (6)	0.0365 (4)	0.0314 (4)	0.0349 (5)	0.0004 (4)	0.0037 (3)
F5	0.0397 (5)	0.0235 (4)	0.0326 (4)	0.0010 (3)	−0.0060 (3)	0.0105 (3)
F6	0.0365 (4)	0.0294 (4)	0.0184 (3)	0.0161 (3)	−0.0027 (3)	−0.0016 (2)
F7	0.0539 (7)	0.0316 (5)	0.0736 (7)	0.0250 (5)	0.0042 (6)	0.0185 (5)
F8	0.0804 (8)	0.0763 (8)	0.0223 (3)	0.0628 (8)	0.0049 (4)	0.0094 (4)
F9	0.0467 (6)	0.0638 (7)	0.0391 (4)	0.0448 (5)	0.0029 (4)	0.0113 (4)
F16	0.0390 (6)	0.0806 (9)	0.0494 (6)	0.0409 (6)	−0.0147 (4)	−0.0076 (5)
F17	0.0812 (9)	0.0436 (6)	0.0433 (5)	0.0428 (6)	−0.0288 (5)	−0.0067 (4)
F18	0.0609 (7)	0.0532 (6)	0.0224 (3)	0.0375 (5)	−0.0125 (4)	−0.0063 (3)
C10	0.0213 (5)	0.0445 (8)	0.0252 (5)	0.0092 (5)	0.0044 (4)	0.0076 (5)
F10	0.042 (2)	0.051 (2)	0.0433 (11)	−0.0210 (13)	0.0068 (14)	0.0037 (15)
F11	0.041 (2)	0.122 (5)	0.053 (2)	0.052 (3)	0.0277 (18)	0.041 (3)
F12	0.038 (2)	0.052 (2)	0.0236 (16)	0.0195 (17)	0.0078 (12)	0.0118 (14)
F10X	0.037 (5)	0.024 (3)	0.059 (7)	0.008 (4)	0.024 (5)	0.012 (3)
F11X	0.014 (3)	0.059 (5)	0.035 (3)	0.014 (3)	0.010 (2)	0.010 (3)
F12X	0.025 (5)	0.056 (7)	0.017 (4)	0.006 (5)	−0.004 (3)	0.001 (4)
C11	0.0353 (7)	0.0193 (5)	0.0298 (5)	0.0077 (5)	−0.0107 (5)	−0.0007 (4)
F13	0.0289 (17)	0.041 (3)	0.089 (4)	−0.0027 (16)	−0.0170 (19)	−0.018 (2)
F14	0.096 (5)	0.0239 (17)	0.037 (3)	0.026 (3)	−0.025 (3)	−0.0060 (19)
F15	0.046 (3)	0.0241 (17)	0.0214 (16)	0.0097 (17)	−0.0106 (18)	−0.0024 (11)
F13X	0.0328 (19)	0.031 (2)	0.040 (3)	0.0009 (14)	−0.0032 (14)	−0.0002 (14)
F14X	0.058 (3)	0.0233 (17)	0.030 (2)	0.0233 (16)	−0.0156 (18)	−0.0048 (14)
F15X	0.059 (6)	0.026 (3)	0.035 (3)	0.015 (3)	−0.027 (3)	−0.0035 (15)

Geometric parameters (Å, º)

Fe1—O1	1.9914 (8)	C5—F4	1.3373 (16)
Fe1—O1^{i}	1.9914 (8)	C5—F5	1.3323 (15)

Fe1—O1^{ii}	1.9914 (8)	C5—F6	1.3289 (13)
Fe1—O2	2.0070 (8)	C6—C7	1.5307 (16)
Fe1—O2^{ii}	2.0070 (8)	C6—F7	1.332 (2)
Fe1—O2^{i}	2.0069 (8)	C6—F8	1.3277 (16)
Fe2—O3^{iii}	1.9866 (8)	C6—F9	1.3257 (17)
Fe2—O3^{iv}	1.9866 (8)	C7—C8	1.3912 (16)
Fe2—O3	1.9866 (8)	C8—H8	0.9500
Fe2—O4^{iii}	1.9997 (8)	C8—C9	1.3944 (16)
Fe2—O4	1.9997 (8)	C9—C10	1.5357 (17)
Fe2—O4^{iv}	1.9997 (8)	C12—C13	1.3945 (16)
Fe3—O5	1.9948 (9)	C12—C11	1.5376 (17)
Fe3—O5^{v}	1.9948 (9)	C13—H13	0.9500
Fe3—O5^{vi}	1.9948 (9)	C13—C14	1.3901 (17)
Fe3—O6^{vi}	2.0012 (9)	C14—C15	1.5414 (17)
Fe3—O6	2.0012 (9)	C15—F16	1.331 (2)
Fe3—O6^{v}	2.0012 (9)	C15—F17	1.3291 (19)
O1—C2	1.2618 (13)	C15—F18	1.3273 (16)
O2—C4	1.2575 (14)	C10—F10	1.302 (6)
O3—C7	1.2597 (14)	C10—F11	1.337 (6)
O4—C9	1.2561 (15)	C10—F12	1.319 (4)
O5—C12	1.2602 (15)	C10—F10X	1.383 (10)
O6—C14	1.2587 (16)	C10—F11X	1.307 (11)
C1—C2	1.5387 (15)	C10—F12X	1.337 (10)
C1—F1	1.3261 (14)	C11—F13	1.371 (9)
C1—F2	1.3283 (16)	C11—F14	1.303 (8)
C1—F3	1.3234 (15)	C11—F15	1.333 (7)
C2—C3	1.3972 (15)	C11—F13X	1.298 (7)
C3—H3	0.9500	C11—F14X	1.349 (7)
C3—C4	1.3938 (15)	C11—F15X	1.312 (9)
C4—C5	1.5395 (15)		

O1—Fe1—O1^{i}	92.74 (3)	O2—C4—C3	127.57 (10)
O1—Fe1—O1^{ii}	92.74 (3)	O2—C4—C5	113.27 (9)
O1^{i}—Fe1—O1^{ii}	92.74 (3)	C3—C4—C5	119.09 (10)
O1^{i}—Fe1—O2	175.07 (3)	F4—C5—C4	109.94 (10)
O1^{ii}—Fe1—O2^{ii}	86.68 (3)	F5—C5—C4	112.21 (10)
O1—Fe1—O2^{ii}	175.07 (3)	F5—C5—F4	107.68 (11)
O1^{ii}—Fe1—O2	92.17 (3)	F6—C5—C4	111.19 (9)
O1—Fe1—O2^{i}	92.17 (3)	F6—C5—F4	107.67 (10)
O1^{i}—Fe1—O2^{ii}	92.17 (3)	F6—C5—F5	107.98 (10)
O1^{i}—Fe1—O2^{i}	86.69 (3)	F7—C6—C7	109.67 (11)
O1^{ii}—Fe1—O2^{i}	175.07 (3)	F8—C6—C7	110.93 (11)
O1—Fe1—O2	86.68 (3)	F8—C6—F7	107.67 (13)
O2^{i}—Fe1—O2^{ii}	88.45 (4)	F9—C6—C7	113.01 (11)
O2^{i}—Fe1—O2	88.45 (4)	F9—C6—F7	106.93 (12)
O2—Fe1—O2^{ii}	88.45 (4)	F9—C6—F8	108.42 (12)
O3^{iii}—Fe2—O3^{iv}	92.73 (3)	O3—C7—C6	113.41 (10)
O3^{iii}—Fe2—O3	92.73 (3)	O3—C7—C8	127.82 (10)

O3^{iv}—Fe2—O3	92.73 (3)	C8—C7—C6	118.77 (11)
O3^{iv}—Fe2—O4	176.31 (4)	C7—C8—H8	120.0
O3—Fe2—O4^{iv}	90.95 (4)	C7—C8—C9	120.06 (11)
O3^{iii}—Fe2—O4^{iv}	176.31 (4)	C9—C8—H8	120.0
O3—Fe2—O4	87.36 (4)	O4—C9—C8	127.58 (10)
O3^{iii}—Fe2—O4^{iii}	87.36 (4)	O4—C9—C10	113.55 (11)
O3^{iv}—Fe2—O4^{iv}	87.36 (4)	C8—C9—C10	118.83 (11)
O3^{iv}—Fe2—O4^{iii}	90.95 (4)	O5—C12—C13	127.78 (11)
O3—Fe2—O4^{iii}	176.31 (4)	O5—C12—C11	114.33 (10)
O3^{iii}—Fe2—O4	90.95 (4)	C13—C12—C11	117.87 (11)
O4^{iii}—Fe2—O4^{iv}	88.95 (4)	C12—C13—H13	120.1
O4^{iii}—Fe2—O4	88.95 (4)	C14—C13—C12	119.84 (11)
O4—Fe2—O4^{iv}	88.95 (4)	C14—C13—H13	120.1
O5^{vi}—Fe3—O5	92.30 (3)	O6—C14—C13	127.93 (11)
O5^{vi}—Fe3—O5^{v}	92.30 (3)	O6—C14—C15	113.77 (11)
O5—Fe3—O5^{v}	92.30 (3)	C13—C14—C15	118.29 (12)
O5—Fe3—O6^{vi}	90.99 (4)	F16—C15—C14	109.73 (13)
O5^{v}—Fe3—O6	90.99 (4)	F17—C15—C14	112.22 (12)
O5^{vi}—Fe3—O6	176.66 (4)	F17—C15—F16	108.17 (13)
O5^{v}—Fe3—O6^{vi}	176.66 (4)	F18—C15—C14	110.69 (11)
O5^{vi}—Fe3—O6^{v}	90.99 (4)	F18—C15—F16	107.46 (13)
O5—Fe3—O6	87.01 (4)	F18—C15—F17	108.42 (13)
O5—Fe3—O6^{v}	176.66 (4)	F10—C10—C9	109.8 (3)
O5^{v}—Fe3—O6^{v}	87.01 (4)	F10—C10—F11	108.8 (4)
O5^{vi}—Fe3—O6^{vi}	87.00 (4)	F10—C10—F12	109.6 (6)
O6^{v}—Fe3—O6	89.74 (4)	F11—C10—C9	110.7 (4)
O6^{v}—Fe3—O6^{vi}	89.74 (4)	F12—C10—C9	110.9 (3)
O6^{vi}—Fe3—O6	89.74 (4)	F12—C10—F11	107.0 (6)
C2—O1—Fe1	128.12 (7)	F10X—C10—C9	107.3 (7)
C4—O2—Fe1	128.00 (7)	F11X—C10—C9	116.8 (8)
C7—O3—Fe2	128.11 (7)	F11X—C10—F10X	106.7 (8)
C9—O4—Fe2	128.22 (8)	F11X—C10—F12X	110.3 (15)
C12—O5—Fe3	128.45 (7)	F12X—C10—C9	112.4 (9)
C14—O6—Fe3	128.43 (8)	F12X—C10—F10X	102.1 (14)
F1—C1—C2	111.33 (9)	F13—C11—C12	106.7 (5)
F1—C1—F2	106.76 (11)	F14—C11—C12	112.4 (5)
F2—C1—C2	109.92 (10)	F14—C11—F13	107.4 (7)
F3—C1—C2	112.61 (10)	F14—C11—F15	112.8 (10)
F3—C1—F1	108.37 (11)	F15—C11—C12	108.7 (6)
F3—C1—F2	107.61 (11)	F15—C11—F13	108.5 (8)
O1—C2—C1	113.79 (9)	F13X—C11—C12	112.0 (4)
O1—C2—C3	127.66 (10)	F13X—C11—F14X	106.5 (7)
C3—C2—C1	118.55 (10)	F13X—C11—F15X	106.2 (10)
C2—C3—H3	120.1	F14X—C11—C12	112.6 (5)
C4—C3—C2	119.72 (10)	F15X—C11—C12	113.9 (8)
C4—C3—H3	120.1	F15X—C11—F14X	105.1 (8)
Fe1—O1—C2—C1	171.13 (7)	C3—C4—C5—F4	109.87 (12)

Fe1—O1—C2—C3	−8.62 (17)	C3—C4—C5—F5	−9.94 (15)
Fe1—O2—C4—C3	8.13 (17)	C3—C4—C5—F6	−130.99 (11)
Fe1—O2—C4—C5	−174.91 (7)	C6—C7—C8—C9	179.53 (11)
Fe2—O3—C7—C6	171.79 (9)	C7—C8—C9—O4	3.6 (2)
Fe2—O3—C7—C8	−8.30 (19)	C7—C8—C9—C10	−173.93 (12)
Fe2—O4—C9—C8	2.16 (19)	C8—C9—C10—F10	105.5 (6)
Fe2—O4—C9—C10	179.82 (9)	C8—C9—C10—F11	−14.6 (7)
Fe3—O5—C12—C13	−7.4 (2)	C8—C9—C10—F12	−133.2 (5)
Fe3—O5—C12—C11	170.74 (9)	C8—C9—C10—F10X	120.1 (9)
Fe3—O6—C14—C13	3.3 (2)	C8—C9—C10—F11X	0.5 (7)
Fe3—O6—C14—C15	−178.22 (9)	C8—C9—C10—F12X	−128.5 (15)
O1—C2—C3—C4	−4.25 (18)	C12—C13—C14—O6	1.0 (2)
O2—C4—C5—F4	−67.38 (12)	C12—C13—C14—C15	−177.39 (12)
O2—C4—C5—F5	172.82 (10)	C13—C12—C11—F13	102.2 (8)
O2—C4—C5—F6	51.76 (14)	C13—C12—C11—F14	−15.4 (11)
O3—C7—C8—C9	−0.4 (2)	C13—C12—C11—F15	−141.0 (7)
O4—C9—C10—F10	−72.3 (6)	C13—C12—C11—F13X	91.4 (6)
O4—C9—C10—F11	167.5 (6)	C13—C12—C11—F14X	−28.6 (6)
O4—C9—C10—F12	48.9 (5)	C13—C12—C11—F15X	−148.2 (10)
O4—C9—C10—F10X	−57.8 (9)	C13—C14—C15—F16	105.36 (15)
O4—C9—C10—F11X	−177.4 (7)	C13—C14—C15—F17	−14.92 (19)
O4—C9—C10—F12X	53.7 (15)	C13—C14—C15—F18	−136.20 (13)
O5—C12—C13—C14	1.1 (2)	F1—C1—C2—O1	41.99 (14)
O5—C12—C11—F13	−76.1 (8)	F1—C1—C2—C3	−138.24 (11)
O5—C12—C11—F14	166.3 (11)	F2—C1—C2—O1	−76.10 (13)
O5—C12—C11—F15	40.7 (7)	F2—C1—C2—C3	103.68 (13)
O5—C12—C11—F13X	−86.9 (6)	F3—C1—C2—O1	163.93 (11)
O5—C12—C11—F14X	153.1 (6)	F3—C1—C2—C3	−16.29 (16)
O5—C12—C11—F15X	33.5 (10)	F7—C6—C7—O3	−67.09 (14)
O6—C14—C15—F16	−73.28 (15)	F7—C6—C7—C8	112.99 (14)
O6—C14—C15—F17	166.44 (13)	F8—C6—C7—O3	51.71 (17)
O6—C14—C15—F18	45.16 (18)	F8—C6—C7—C8	−128.21 (13)
C1—C2—C3—C4	176.01 (10)	F9—C6—C7—O3	173.72 (12)
C2—C3—C4—O2	4.45 (18)	F9—C6—C7—C8	−6.20 (18)
C2—C3—C4—C5	−172.36 (10)	C11—C12—C13—C14	−176.92 (12)

Symmetry codes: (i) −*x*+*y*+1, −*x*+2, *z*; (ii) −*y*+2, *x*−*y*+1, *z*; (iii) −*y*+1, *x*−*y*, *z*; (iv) −*x*+*y*+1, −*x*+1, *z*; (v) −*y*+1, *x*−*y*+1, *z*; (vi) −*x*+*y*, −*x*+1, *z*.